Multimodal classification of neurons in the lateral septum

Christopher M. Reid[1,2,3,4], Yuqi Ren[1,2], Yajun Xie[1,2], Miguel Turrero García[1,2], Diana Tran[4], Steve Vu[4], Jonathan Liu[5], Manal A. Adam[1,2], Sarah M. Hanson[1,2], Angela O. Pisco[5], Corey C. Harwell[1,2,5,6,7*]

[1]Department of Neurology, University of California, San Francisco, CA

[2]Eli and Edythe Broad Center of Regeneration Medicine and Stem Cell Research, San Francisco, CA

[3]Program in Neuroscience, Harvard Medical School, Boston, MA

[4]Department of Neurobiology, Harvard Medical School, Boston, MA

[5]Chan Zuckerberg Biohub San Francisco, San Francisco, CA

[6]Weill Institute for Neurosciences, University of California, San Francisco, CA

[7]Lead contact

*Correspondence: Corey.harwell@ucsf.edu

ABSTRACT

The lateral septum (LS) is a nucleus in the ventral forebrain that modulates complex social and affective behaviors. Several distinct neuronal types have been described in the LS; however, the full extent of this cellular and molecular diversity remains unclear. We address this gap by profiling the transcriptional identity of mature LS neurons originating from two progenitor lineages defined by their anatomical location and expression of the transcription factor *Nkx2.1*. We describe 12 molecularly distinct subtypes of LS neurons that fall into two main groups: those with a history of *Nkx2.1* expression and those without. We discovered that LS neurons from the *Nkx2.1* lineage share an enrichment of select cell adhesion and communication molecules. Despite this, we found that LS neurons that have distinct developmental origins can exhibit significant transcriptional similarities. We then examined the spatial relationships among neurons in the LS, revealing that each subtype occupies a discrete anatomical domain. These anatomical domains are defined by graded patterns of gene expression that correlate with the molecular taxonomy of LS neuron subtypes and encode proteins involved in synaptic signaling. Lastly, we genetically labeled non-overlapping subgroups of LS neurons, and detailed their connective, morphological, and electrophysiological properties. Our findings offer a deeper understanding of neuronal heterogeneity in the LS, paving the way for future studies into how these neuronal types contribute to regulating emotional and motivated behaviors.

INTRODUCTION

The ability to properly regulate affective and motivated behaviors is a fundamental requirement for social interaction and effective decision-making. These behaviors are orchestrated by a complex network of structures collectively known as the limbic system (Catani et al., 2013; Rajmohan and Mohandas, 2007; Sheehan et al., 2004; Sokolowski and Corbin, 2012). A complete understanding of how this system operates in diseased and healthy states requires a comprehensive knowledge of the cell types and circuitry within limbic structures. The lateral septum (LS) is a ventral forebrain region within the limbic system that plays a pivotal role in regulating complex affective, motivated, and social behaviors (Besnard and Leroy, 2022; Menon et al., 2022; Rizzi-Wise and Wang, 2021; Sheehan et al., 2004; Wirtshafter and Wilson, 2021). Compared to other limbic regions such as the cortex, hippocampus, and hypothalamus, our knowledge of the cell types present in the LS is limited (Cembrowski et al., 2016; Kim et al., 2020; Moffitt et al., 2018; Zeisel et al., 2015).

The LS is primarily composed of GABAergic projection neurons which have historically been classified based on their morphological and physiological properties, as well as their anatomical connections (Alonso and Frotscher, 1989; Gallagher et al., 1995a; Leranth and Frotscher, 1989; Risold and Swanson, 1997). These features have been used to subdivide the LS into three distinct nuclei: the lateral septum dorsal (LSd), the lateral septal intermediate (LSi), and the lateral septum ventral (LSv). Inputs coming from the hippocampus are topographically organized, with neurons located in dorsal areas projecting to the LSd and those ventral regions projecting to the LSv. Similarly, fibers projecting from the LS to diencephalic and subpallial structures typically follow a lateral-to-medial trajectory, with the LSd projecting laterally and the LSv projecting medially (Raisman, 1966; Risold and Swanson, 1997; Swanson and Cowan, 1979).

Recently, groups of functionally distinct LS neurons have been characterized based on differences in the expression of neuropeptides and neurotransmitter receptors. For instance, somatostatin (*Sst)* expressing neurons in the LSd have been implicated in the regulation of context-associated fear behaviors and are thought to be anxiolytic (An et al., 2022; Besnard et al., 2019; Li et al., 2022). In contrast, neurons expressing the corticotropin releasing hormone receptor 2 (*Crhr2*) in the LSi are activated by threatening stimuli and are anxiogenic (Anthony et al., 2014; Hashimoto et al., 2022). In the rostral LS, a group of neurotensin *Nts* expressing neurons were shown to modulate social behaviors and gate hedonistic feeding behaviors (Azevedo et al., 2020; Chen et al., 2022; Li et al., 2023). Collectively, these findings highlight the functional heterogeneity of LS neurons; however, a proper characterization of defined neuronal types requires a multimodal examination of their cell biological properties (Gouwens et al., 2020; Zeng, 2022).

Observations from well-studied areas of the brain such as the cortex, have shown that the taxonomy of neurons within a region often corresponds to their developmental origins (Mayer et al., 2018; Tasic et al., 2016; Yao et al., 2021). The septal proliferative zone is characterized by the expression of ZIC family transcription factors (Gaston-Massuet et al., 2005; Inoue et al., 2007; Magno et al., 2017; Turrero García et al., 2021). Within this zone, progenitors in the caudal part of the embryonic septum—termed the septal eminence—can be differentiated from their rostral counterparts by the expression of the transcription factor *Nkx2.1* (Magno et al., 2017; Turrero García et al., 2023, 2021; Wei et al., 2012). *Nkx2.1* is most prominently known to be expressed in the medial ganglionic eminence—a region adjacent to the embryonic septum—where it is critical for the development of forebrain interneurons (Flames et al., 2007; Mayer et al., 2018; Sandberg et al., 2016; Turrero García and Harwell, 2017). Moreover, a loss of *Nkx2.1* in the septal eminence results in a severe depletion of medial septal and globus pallidus cholinergic neurons born from there (Magno et al., 2017). We previously described a subset of LS neurons that originate from the septal eminence, are morphologically heterogeneous and necessary for the proper execution of threat response behaviors (Turrero García et al., 2023, 2021). Taken together, these prior studies suggest that LS neurons with a developmental history of *Nkx2.1* expression may exhibit characteristics that distinguish them from those derived from the rostral embryonic septum.

In this study, we identified 12 transcriptionally distinct subtypes of LS neurons, which can largely be divided into two groups based on their developmental expression of *Nkx2.1*. We show that while neurons from the same lineage express common sets of cell adhesion and cell communication molecules, ultimately developmental history does not predict molecular taxonomy. Additionally, we show that LS neuron subtypes are discretely organized into distinct domains along the dorsal-ventral and rostral-caudal axes of the septum. Furthermore, the transcriptional relationships between subtypes are defined by patterns of gene expression that correlate with the anatomy of the LS. Leveraging our transcriptomic data, we identified markers that can be used to characterize anatomical and physiological attributes of genetically defined non-overlapping subgroups of LS neurons. Collectively, this research provides a comprehensive examination of neuronal heterogeneity within the LS and lays the foundation for targeted functional studies.

RESULTS

Molecular taxonomy of developmentally defined lateral septal neuron subtypes

We reasoned that lateral septal neuron (LSNs) derived from *Nkx2.1* expressing progenitors in the septal eminence may share cellular and molecular characteristics that correspond to their lineage origin (Sandberg et al., 2016; Turrero García et al., 2021; Wei et al., 2012). We labeled neurons with a developmental history of *Nkx2.1* expression by crossing Nkx2.1-Cre mice with animals carrying an allele encoding a Cre-dependent red fluorescent protein (RFP), tdTomato. This marked a subset of LSNs

(Nkx2.1+ LSNs) that were found in all anatomical regions of the LS and were positive for the ZIC transcription factors (**Figure 1A, S1A**). Using the neuronal marker NeuN, we quantified the total proportion of LSNs that were RFP positive (22.7%), as well as their enrichment across the dorsal, intermediate, and ventral subregions of the LS (LSd: 11.7%, LSi: 29.2%, LSd: 29.7%) (**Figure 1B**). We also assessed the proportion of RFP positive LSNs across four coronal sections along the anterior-posterior axis, finding them to be more concentrated in intermediate areas (Section 1: 15.4%, Section 2: 31.0%, Section 3: 27.3%, Section 4: 13.01%). A small fraction of Nkx2.1+ LSNs (11.8%) were not positive for the ZIC transcription factors (**Figure S1B**), suggesting that they might originate from *Nkx2.1* expressing progenitors located outside the embryonic septum, such as the medial ganglionic eminence or preoptic areas (Azzarelli et al., 2015; Mayer et al., 2018; Turrero García and Harwell, 2017; Wei et al., 2012).

To determine if a *Nkx2.1* expression history distinguishes a unique subgroup of LSNs, we developed an experimental strategy to profile the transcriptional identity of LSNs while preserving information about their developmental origins (**Figure 1C**). We dissected the septum of adult Nkx2.1-Cre mice carrying a conditional Sun1GFP allele for Cre-dependent labeling of the nuclear membrane (Mo et al., 2015). We then isolated the nuclei of septal cells and used fluorescent activated nuclei sorting (FANS) to separate GFP-positive and negative nuclei. Subsequently we performed single nucleus RNA-seq (snRNA-seq) on each sorted population and obtained a total of 25,173 cells that expressed an average of 3,014 unique genes. Using principal component analysis (PCA) we constructed a neighborhood graph which allowed us to visualize the data in two dimensions. Our sequencing approach enabled us to distinguish between GFP-positive cells, indicating a history of *Nkx2.1* expression (Nkx2.1+) and GFP-negative cells that had never expressed *Nkx2.1* (Nkx2.1-) (**Figure 1D**).

We applied unsupervised Leiden clustering at several resolutions to understand the relationships between the groups of cells (**Figure S2A**). Using a Leiden resolution of 0.9, we performed differential gene expression analysis and identified genes that were uniquely enriched within each cluster (**Figure S2B**). We combined this gene list with established cell type markers—such as *Rbfox3* (neurons), *Aldh1l1* (astrocytes), and *Mobp* (oligodendrocytes)—as well as markers indicative of developmental origin like *Nkx2.1*, *Zic1*, and *Lhx8* (Mayer et al., 2018; Turrero García et al., 2021; Turrero García and Harwell, 2017; Yao et al., 2023). We determined the regional expression pattern of each marker using the Allen Brain Atlas *in situ* resource (Lein et al., 2007) and annotated 14 distinct cell groups (**Figure 1E**). Our dissection methods captured cells from regions outside of the LS, such as medial septal neurons (MSNs), triangular septal neurons (TRNs), and striatal neurons (StrNs). Consistent with previous studies, we found that the majority of MSNs (93.6%) have a history of *Nkx2.1* expression (**Figure S2C**) (Magno et al., 2017; Wei et al., 2012). Notably, we observed a sharp contrast in *Nkx2.1* lineage between medial and lateral septal astrocytes—at 87.2% and 10.8% respectively—indicating that astrocytes in the septum have distinct developmental origins (Xie et al., 2023).

We subclustered the 5,103 LSNs, which were primarily defined by their enriched expression of *Myo5b*, *Trpc4*, and *Prdm16* (Tian et al., 2014; Turrero García et al., 2021). UMAP analysis of their lineage identities revealed a clear segregation between Nkx2.1+ and Nkx2.1+- LSNs (**Figure 1F**). To assess the heterogeneity of LSNs we employed Leiden clustering at various resolutions to aid our annotation of 12 transcriptionally distinct subtypes (**Figure S2D, 1G**). We identified the minimal markers necessary to identify each subtype (**Figure 1H**), noting that many previously recognized markers, such as *Sst*, *Crhr2*, *Drd3*, and *Nts*, were selectively expressed by specific LSN subtypes (**Figure 1I)**(Anthony et al., 2014; Besnard and Leroy, 2022; Chen et al., 2022; Shin et al., 2018). Each subtype was defined by a unique combination of enriched genes (**Figure 1J**), and predominantly consisted of either Nkx2.1+ or Nkx2.1- cells, except for LSN-2, which had a near equivalent distribution from both groups (57.2% Nkx2.1+) (**Figure 1K**). We used the total average gene expression to hierarchically cluster the cell groups (**Figure 1K**), discovering that some Nkx2.1+ subtypes were more transcriptionally related to Nkx2.1- subtypes, specifically LSN-1 to LSN-3, LSN-6 to LSN-8, and LSN-5 to LSN-12. Collectively, these results demonstrate that the LS contains multiple transcriptionally distinct neuronal populations, and that developmental origin alone cannot define their molecular taxonomy.

Nkx2.1 lineage neurons share expression of select cell adhesion and communication genes

To explore the transcriptional features distinguishing Nkx2.1+ from Nkx2.1- LSNs, we conducted a pairwise differential gene expression analysis between the two groups, revealing 683 differentially expressed genes (**Figure 2A**). We found that the long non-coding RNA *Sfta3-ps* is highly enriched in Nkx2.1+ cells in a similar pattern to *Nkx2.1*, whereas the transcription factor gene *Meis2* is predominantly expressed in Nkx2.1- cells (**Figure 2B**). The mutually exclusive expression patterns of the two genes reflected the developmental origins of the LSNs born from either the rostral or caudal embryonic septum, dividing the subtypes into two groups: those that express *Meis2* and those expressing *Sfta3-ps* (**Figure 2C**).

We then explored the regulatory pathways active in LSNs using the single-cell regulatory network inference and clustering (SCENIC) computational method, allowing us to infer which transcription factor-target regulatory networks—known as regulons—were specifically active in either Nkx2.1+ or Nkx2.1- LSNs (Aibar et al., 2017). From this analysis, the NKX2.1 regulon was predicted to be specifically enriched in Nkx2.1+ LSNs, while the RARB regulon was enriched in Nkx2.1- LSNs (**Figure S3A, Table S1**). The combined expression pattern of inferred target genes for NKX2.1 and RARB paralleled the differences in *Nkx2.1* lineage identities among the LSNs (**Figure 2D**). Interestingly, several of the top differentially expressed genes distinguishing Nkx2.1+ from Nkx2.1- LSNs were predicted targets of either NKX2.1 or RARB **(Figure 2E**). For instance, *Slit2*, which encodes a secreted glycoprotein critical for axon guidance (Ba-Charvet et al., 1999; Bagri et al., 2002; Gonda et al., 2020), is highly expressed in Nkx2.1+

neurons, whereas *Sorcs2*, a gene encoding a proBDNF receptor important for synaptic plasticity (Glerup et al., 2016), is predominantly expressed in Nkx2.1- neurons.

Following this, we performed gene ontology (GO) analysis to describe the molecular function of the top differentially expressed genes (**Figure 2F, Table S2**). Notably, the significant terms associated with genes enriched in Nkx2.1+ neurons encoded proteins central to cell adhesion and signaling pathways, and included genes such as *Ntng1*, *Nrxn1*, and *Nrg.* In contrast, the genes enriched in Nkx2.1- LSNs were associated with terms related to synaptic signaling and ion channel regulation, of which the most significant being “calcium channel activity”, including the genes *Grm7*, *Cachd1*, *Cacnb2,* and *Ryr2*. Taken together, these findings indicate that Nkx2.1+ LSNs operate under gene regulatory pathways distinct from Nkx2.1- LSNs and are uniquely defined by the expression of select cell adhesion and communication molecules.

Transcriptionally distinct subtypes of lateral septal neurons reside in unique anatomical domains

Our hierarchical clustering of fate mapped LSNs suggests that developmental origin alone is not sufficient to define their molecular taxonomy. Given this, we sought to identify the shared transcriptomic features of LSN subtypes with distinct developmental origins, focusing on three pairs of subtypes that comprised transcriptionally related yet developmentally distinct neurons: LSN-1 and LSN-3, LSN-6 and LSN-8, and LSN-5 and LSN-12. We conducted a pairwise differential gene analysis between each pair and all other LSNs, focusing on the top differentially expressed genes (**Figure S4A**). Interestingly, many of the genes enriched within the paired subtypes exhibited a graded pattern of expression among LSNs (**Figure S4B**). Given that the circuitry and functional specialization of the LS is topographically organized (Besnard and Leroy, 2022; Risold and Swanson, 1997; Sheehan et al., 2004), we hypothesized that these transcriptional features were linked to the spatial allocation of the LSN subtypes.

To investigate the relationship between the anatomical distribution of LSN subtypes and their transcriptional profiles, we performed spatial transcriptomics using MERFISH on coronal sections of P35 septum across 2 replicates (**Figure 3A**). We constructed a 500-gene panel by identifying the minimum number of genes necessary to define each LSN subtype using a one-versus-all random forest classifier on our snRNA-seq dataset (Park et al., 2020). We supplemented this list with genes that defined the transcriptionally similar pairs, as well as markers of MSNs, and non-neuronal cell types. After processing the samples, we found that a total of 263,947 cells passed our quality control filters. We then applied the same dimensionality reduction and clustering analysis as previously described. (**Figure S5A**). Using established markers (**Figure S5B**), we subclustered 44,715 LSNs and annotated the same 12 transcriptionally distinct LSN subtypes defined in the snRNA-seq data (**Figure 3B**). When comparing the transcriptional profiles of LSN clusters between the MERFISH and snRNA-seq datasets, we observed an average Pearson correlation of 0.81, indicating that they represent identical subtypes (**Figure 3C**).

Subsequently, we selected five sections representing different regions along the anterior-posterior axis of the septum and plotted the spatial organization of each LSN subtype (**Figure 3D**). This revealed that the LSN subtypes are arranged as nuclei layered in an onion skin-like pattern, as previously described (Besnard and Leroy, 2022; Turrero García et al., 2021; Wei et al., 2012) . Each subtype predominantly occupied a specific anatomical domain; for instance, LSN-4 was primarily found in dorsal regions, whereas LSN-7 was confined to medial areas. Notably, some groups, such as the transcriptionally similar pair LSN-5 and 12, exhibited a considerable overlap in their spatial distribution. Furthermore, the high cell counts of the MERFISH data revealed an additional layer of heterogeneity within the cell groups. Specifically, subtypes 1, 4, 6, and 7 could each be further divided, with those from LSN-4 being the most numerous neuronal type in the LS (**Figure 3E, 3F**). This finer resolution of subtype identity often correlated with differences in their anatomical position along the dorsal-ventral axis (**Figure 3G**). Moreover, some of the marker genes that defined the secondary groups were expressed among multiple cardinal subtypes; notable examples include *Met*, *Robo2*, and *Sall3* **(Figure 3H)**. Together, these findings provide a comprehensive transcriptomic and spatial atlas of defined neuronal types in the LS.

Spatially variable genes define the molecular identity of lateral septal neurons

Having mapped the spatial organization of the neuronal clusters, we could then explore the relationship between their anatomical position, molecular profile, and developmental origin. We used the spatial coordinates of cells from the MERFISH dataset to score the proximity between the subtypes. This approach enabled us to hierarchically cluster the groups based on their anatomical closeness (**Figure S6A**). We compared the resulting dendrogram to the one constructed using the average gene expression profiles from the snRNA-seq dataset (**Figure 1L**). From this, we found that several LSN subtypes exhibited a spatial relationship that paralleled their molecular taxonomy. For instance, LSN-5 and 12 are transcriptionally similar and occupy an overlapping anatomical domain (**Figure S6B**). Additionally, these two groups have distinct developmental origins, suggesting that factors related to their spatial allocation drive them to become transcriptionally related.

Similarly, LSN-6, 8, and 10 cluster together based on their transcriptional features and reside in adjacent anatomical regions. However, some groups that had related molecular profiles showed a low neighborhood enrichment, such as LSN-1 and 3 **(Figure S6B)**. Given this, we shifted our focus towards understanding whether the genes that are enriched among LSN subtypes from different lineages are related to their anatomical positioning. To achieve this, we used the statistical tool SpatialDE (Svensson et al., 2018) on our MERFISH dataset to unbiasedly identify 134 spatially variable genes (SVGs)—genes expressed in gradient patterns that were independent of subtype. Many SVGs exhibited similar patterns of gene expression (**Figure S6C**), and could be grouped into eight major gene sets, each characterizing a unique anatomical region of the LS: Dorsal-Lateral, Dorsal-Medial, Dorsal-Medial Inverse, Ventral, Ventral-Rostral, Ventral-Caudal, Lateral, and Medial (**Figure 4A, 4B**).

Notably, the expression profile of these SVG patterns across the LSN subtypes largely reflected their molecular taxonomy (**Figure 4C**). For example, both LSN-6 and 8 highly express Dorsal-Medial genes and lack expression of Dorsal-Medial Inverse genes; in contrast, LSN-5 and 12 primarily express Ventral and Ventral-Caudal genes. We used GO analysis to investigate the functions of SVGs and found that many of them are involved in synaptic signaling and activity dependent calcium regulation. (**Figure 4D**). For example, LSN-6 and 8 shared a high expression of the calcium-permeable channels *Chrne*, *Trpc3*, *Itpr3*, and *Ryr3*, as well as the calcium-dependent channels *Ano2* and *Kcnn3* (**Figure 4E**). Likewise, both LSN-1 and 3 highly express the NMDA receptor *Grin3a* and the calcium-transporting ATPase *Atp2b* (Seal et al., 2023). Considering that a significant portion of SVGs play a role in the calcium signaling pathway, it is possible that groups of neurons co-expressing these genes share similar electrophysiological characteristics. In conclusion, these findings suggest that spatial gene expression patterns have a significant role in defining the molecular identity of LSNs regardless of lineage origins.

Electrophysiological and morphological properties of genetically defined lateral septal neurons

Early classifications of LSN were based on their physiological and morphological properties (Alonso and Frotscher, 1989; Gallagher et al., 1995b; Raisman, 1969), yet how these characteristics correlate with their molecular identity remains unclear. To investigate this, we leveraged our sequencing data to identify markers with available genetic tools that label non-overlapping subgroups of LSNs. The graded expression of many septal genes makes the targeting of a single subtype challenging; however, we identified markers that predominantly labeled only one or two subtypes: *Lhx2*, *Esr1*, *Ndnf*, and *Foxp2* (**Figure 5A**). *Foxp2* and *Esr1* are primarily expressed by subtypes LSN-1 and 5, respectively. *Ndnf* is expressed by both LSN-4 and 6, while *Lhx2* is expressed by LSN-8 and LSN-11 (**Figure 5B**). Moreover, the subtypes captured by these markers represented neurons with distinct developmental histories that occupy unique anatomical domains (**Figure 5C**).

We labeled each population by systemic injections of a blood-brain barrier crossing adeno-associated virus (AAV) that expresses a Cre-dependent mCherry reporter into transgenic mouse lines expressing Cre under the control of our selected markers (Challis et al., 2019). This enabled us to target mCherry-positive neurons for whole-cell patch clamp recording followed by filling with neurobiotin to analyze the intrinsic physiological and morphological properties of each group. Each LSN subgroup was morphologically unique and exhibited observable differences in spine density, dendritic thickness, and soma size (**Figure 5D, 5E**). This was accompanied by variations in their intrinsic properties, including their firing type and actional potential waveform (**Figure 5F**). Additionally, they displayed distinctive depolarization, repolarization, and refractory period phases, suggesting underlying differences in ion channel expression (Bean, 2007) (**Figure 5G**). *Ndnf* neurons showed two distinct firing patterns and morphologies dependent upon their topographical location along the medial-lateral axis of the LSd. This separation matched with the anatomical distribution of LSN-4 (lateral) and 6 (medial). At high current

injections, *Esr1*, *Foxp2*, and lateral *Ndnf* neurons fired and sustained a regular sequence of action potentials. In contrast, *Lhx2* and medial *Ndnf* neurons spiked irregularly, each showing a unique firing pattern. *Lhx2* neurons spiked transiently, producing only a few action potentials that had successive reductions in peak amplitude and widening of the spike width. When subjected to high current injections, medial *Ndnf* neurons displayed an erratic firing pattern characterized by a combination of regular spikes and plateau potentials. All groups except for *Ndnf* neurons demonstrated a prominent inward-hyperpolarizing current at negative current injections, a characteristic of inward-rectifying potassium channels (Hibino et al., 2010; Mao et al., 2003).

Using 14 intrinsic parameters collected from the recordings, we compared the electrophysiological profile of each subgroup, and found that *Esr1* and *Foxp2* neurons shared similar intrinsic properties, while *Lhx2* neurons were the most distinct (**Figure 5H**). The electrical properties of neurons are determined by the complement of voltage-gated ion channels that they express (Bean, 2007; Burke and Bender, 2019); using our snRNA-seq dataset, we identified sets of voltage-gated ion channels that were differentially expressed among LSNs. In line with their intrinsic physiological relationships, *Esr1* and *Foxp2* shared a similar enrichment of channels. Notably, *Lhx2* neurons expressed the largest number of uniquely expressed channels, primarily from the voltage-gated potassium channel family (**Figure 5I**).

Anatomical connections of molecularly distinct lateral septal neurons

As a central component of the limbic system, the lateral septum serves as an essential node for information flow between cortical and subcortical structures (Sheehan et al., 2004; Wirtshafter and Wilson, 2021). Considering this, we sought to systematically map the connectivity of molecularly distinct LSNs. The efferent projections of each subgroup were labeled by local injection of an AAV expressing a Cre-dependent eGFP and synaptophysin-fused mRuby, into four LS of each transgenic lines (For more specific labeling, we opted to use the Chat-Cre line—which primarily labels LSN-11—instead of the Lhx2-CreER line) (**Figure 6A, 6B**). The fibers of each subgroup displayed unique projection patterns, targeting distinct hypothalamic, subpallial and midbrain regions (**Figure 6C**).

Esr1 and *Foxp2* neurons exhibited distributed projection patterns targeting various hypothalamic areas, with no single area receiving more than 25% of their total projections. The terminals of both groups highly innervated the medial preoptic area (MPO), a key regulator of energy balance and sexual behaviors (Dulac et al., 2014). In contrast, *Chat* and *Ndnf* neurons showed more restricted projection patterns, with one or two regions accounting for the majority of the total projections. The terminals of *Chat* neurons densely innervated the anterior hypothalamic area (AHN), while *Ndnf* neurons selectively targeted the nucleus of the diagonal band (NDB) and the lateral hypothalamic area (LHA) (**Figure 6D**). Chat-neurons (LSN-11) are a subset of *Crhr2*-expressing LSNs, whose projections to the AHN have been shown to regulate threat-response behaviors (Anthony et al., 2014; Hashimoto et al., 2022). The NDB and LHA are key modulators of cognitive processes, including attention, learning, goal-seeking and memory consolidation (Yamashita and Yamanaka, 2016; Petrovich, 2018; Liu et al., 2018). Collectively, these

findings reveal significant differences in the postsynaptic targets of molecularly distinct LSNs, likely reflective of the behaviors they modulate.

We used mono-synaptic rabies tracing in combination with the same transgenic Cre lines to identify the presynaptic inputs onto genetically defined groups (**Figure 6E**). While each group received inputs from numerous brain regions, the hippocampal subregions contributed the largest proportion (**Figure 6F**), consistent with previous reports (Albert et al., 1978; Gergues et al., 2020; Raisman, 1969; Risold and Swanson, 1997) . The majority of hippocampal inputs onto *Chat* neurons came from the ventral CA1 and CA3 subregions. Similarly, *Foxp2* neurons predominantly received innervation from ventral hippocampus regions, but also received inputs from its dorsal regions. Interestingly, *Esr1* neurons received an even distribution of inputs from the dorsal and ventral hippocampal regions with a higher contribution from the CA3 region than CA1 (28.4% vs. 16.1%). *Ndnf* neurons had the largest proportion of input from the dorsal hippocampus, mostly from CA3 areas.

We categorized the extensive inputs received by each subgroup into nine general areas (**Figure 6G**), emphasizing the proportional differences in afferent connections from each region. In addition to the hippocampus, we observed notable differences in presynaptic labeling in the hypothalamus and LS. *Chat* and *Ndnf* neurons largely received inputs from the medial preoptic hypothalamic regions, while *Esr1* and *Foxp2* neurons were targeted by posterior hypothalamic regions (**Figure 6H**). Within the LS, the majority of retrogradely labeled cells were located in the same subregion as the starter cells (**Figure 6I**). For *Chat* and *Ndnf* neurons, these cells were mostly located laterally to the starter cells, whereas for *Foxp2* and *Esr1* neurons, the LS input cells were somewhat intermingled with starter cells. Together these data provide a comprehensive atlas of the input and output connectivity of non-overlapping genetically defined LSNs.

DISCUSSION

Neurons in the lateral septum (LS) regulate complex affective, social, and motivational processes, and are organized topographically along its anatomical axis (Besnard et al., 2019; Menon et al., 2022; Sheehan et al., 2004; Wirtshafter and Wilson, 2021). A complete understanding of their specialized functional properties requires a characterization of their cellular features across multiple modalities. (Gouwens et al., 2020; Peng et al., 2021; Wang et al., 2023; Zeng, 2022; Zhang et al., 2023). Some of these features are intrinsically encoded through lineage related developmental programs, while others are molded by extrinsic factors from their local environment. In this study, we resolve the multimodal features and organizational principles of lateral septal neurons (LSNs) by detailing their transcriptome, developmental origin, synaptic partners, and physiological properties. We identified 12 molecularly distinct LSNs types that are shaped by both their developmental lineage and anatomical location.

Nkx2.1+ LSNs comprise at least four distinct subtypes that share a common set of transcriptional features. The most prominent feature being the lncNRA *Sfta3-ps,* which distinguishes Nkx2.1+ LSNs from Nkx2.1- LSNs*. Sfta3-ps,* also known as the Nkx2.1-associated noncoding intergenic RNA (NANCI) is located adjacent to *Nkx2.1* in the genome, and is believed to positively regulate the transcription factor (Herriges et al., 2017, 2014; Katayama et al., 2005). The high expression of *Sfta3-ps* may be required for maintaining a low and persistent expression of *Nkx2.1* in mature LSNs, in contrast to cortical interneurons which downregulate the transcription factor post-mitotically (Elias et al., 2008). This sustained expression pattern mirrors neurons in the basal ganglia, suggesting that the post-mitotic expression of *Nkx2.1* in the LS is likely required for proper neuronal migration and wiring. Furthermore, its continued expression in the mature septum may play a crucial role in the maintenance of connections or migratory processes. (Magno et al., 2017; Nóbrega-Pereira et al., 2008). In line with this, our computational analysis identified a set of cell adhesion and communication molecules as downstream effectors of NKX2.1 in mature LSNs.

We identified several genes critical for neurodevelopment as potential targets of NKX2.1, including a gene encoding the axon guidance molecule SLIT2, a key substrate for the formation of gross anatomical connections (Ba-Charvet et al., 1999; Gonda et al., 2020; Hu, 1999; Minocha et al., 2015). A subset of CA3 hippocampal fibers highly express ROBO1, the canonical receptor for SLIT2, and may be subjected to the chemorepulsive effect imposed by *Slit2* expressing Nkx2.1+ LSNs (Alvarez-Buylla, 1997; Blockus et al., 2021; Fouquet et al., 2007). Other putative targets of NKX2.1 may specify the synaptic connections of LSNs, such as the cell adhesion molecule *Netrin-g1,* which promotes the outgrowth of axonal fibers and organizes their distribution along the dendritic arbor (Nishimura-Akiyoshi et al., 2007). Loss of *Netrin-g1* results in a dysregulation of fear and anxiety-like behaviors, a phenotypic hallmark of disruptions in the LS (Nishimura-Akiyoshi et al., 2007, 2007; Short et al., 2023; Zhang et al., 2016).

While our computational analysis was limited to inferring networks of activated genes, the repressive functions of NKX2.1 are well-documented (Sandberg et al., 2016). Notably, NKX2.1 is thought to repress the transcription factor *Meis2* (Sandberg et al., 2016), a gene uniquely expressed in Nkx2.1- LSNs. Historically known for its role in cell fate determination, MEIS2 also functions as a co-factor for other transcriptional regulators (Dupacova et al., 2021; Moens and Selleri, 2006; Su et al., 2022). MEIS2 might interact with transcription factors, such as PAX6 and PBX3, and modulate the expression of genes that define the identity and function of Nkx2.1- LSNs (Agoston et al., 2014; Bobola and Sagerström, 2024). Taken together, the diverse regulatory programs embedded in LSNs by their developmental lineage shape their molecular identities, and potentially contribute to the functional diversity of mature LSN.

Using MERFISH we generated the first comprehensive spatial atlas of transcriptomically defined septal neurons. We demonstrate that LSN subtypes are organized into discrete nuclei layered from the midline, reflecting the onion-skin-like organization of the septum (Wei et al., 2012). This topographic organization can be attributed to the outside-in development of the septum, where early-born neurons are positioned medially, and late-born neurons are stacked laterally (Creps, 1974; Turrero García et al., 2021; Wei et al.,

2012). However, the complex spatial patterning of LSN subtypes is influenced by variations in molecular and functional cell type identities along the rostrocaudal and dorsoventral axis. The parcellation of LSN subtypes along these spatial axes is reminiscent of the multiple progenitor domains that divide the embryonic septum (Flames et al., 2007; Turrero García et al., 2021; Wei et al., 2012). In fact, several genes—most of which are transcription factors—that define the proliferative regions of the septum, including *Pax6*, *Lhx2*, *Zeb2*, and *Nkx2.1*, are expressed in anatomically separated subsets of mature LSNs. An understanding of how the cytoarchitecture and cell biological processes of the developing septum establish the topography of mature LSNs will require a detailed mapping of their clonal relationships (Bandler et al., 2022; Delgado et al., 2022; Harwell et al., 2015; Mayer et al., 2015).

The high resolution of the MERFISH dataset enabled us to further divide several of the principal subtypes (LSN-1, 4, 6, and 7) into more refined groups that are distinguished by their location along the dorsoventral axis of the LS. This additional heterogeneity was largely driven by a subset of spatially variable genes (SVGs) that were often expressed in gradients. We identified eight SVG sets that significantly influence the molecular identity of LSNs, driving developmentally distinct subtypes to adopt similar transcriptional profiles. The anatomical patterns formed by the SVGs largely correspond to the organization of hippocampal excitatory inputs into the LS, underscoring the functional relevance of these genetic signatures. (Besnard and Leroy, 2022; Risold and Swanson, 1997). We found that the majority of SVGs encode post-synaptic proteins that regulate neuronal activity and synaptic transmission. For instance, both LSN-6 and 8 highly express *Grid2ip,* which encodes a glutamate receptor-binding protein that facilitates long-term depression (Sonoda et al., 2006). Similarly, LSN-1 and 3 highly express *Grin3a,* which encodes a NMDA glutamate receptor that mediates postnatal spine development and is implicated in social and mood disorders (Jin et al., 2021; Kehoe et al., 2014). These examples illustrate how groups of LSN subtypes with distinct developmental origins can ultimately exhibit similar transcriptional profiles, indicating a complex interplay between developmental programing and the functional demands of LS.

Conversely, the expression of SVGs can drive developmentally related subtypes to diverge from each other and become transcriptionally dissimilar. For instance, LSN-8 and 11 are two Nkx2.1+ subtypes that uniquely express several genes (*Lhx2*, *Dach2, Tafa1, Crhr2, Lama3, Gpr139*), are morphologically and physiologically identical, yet ultimately are unrelated based on the transcriptomic taxonomy of LSNs. The features that distinguish LSN-8 from LSN-11 are predominantly SVGs that encode proteins involved in synaptic plasticity or signal transduction. Their occupation of separate spatial domains reflects their differential expression of SVGs, with LSN-11 being located ventrally and LSN-8 positioned dorsal-medially. Traditionally, these two subtypes have been considered as a homogenous population based on the expression of the corticotropin-releasing hormone receptor 2 (Crhr2) and their role in regulating threat response behaviors (Anthony et al., 2014; Hashimoto et al., 2022; Turrero García et al., 2023). However, their distinct transcriptomic profiles suggest they may process postsynaptic information differently. The factors driving the expression of SVGs and the dynamic nature of their expression remain unknown.

However, a recent study focusing on LSNs that express Nts revealed that ion channel genes—a gene family prominently featured within the SVG sets—are selectively altered during opioid-induced withdrawal (Simon et al., 2024) . This suggests that the expression of SVGs may be dynamically regulated by external factors that profoundly influence the molecular profile of LSNs and work in concert with intrinsic lineage programs to determine cell identity.

Leveraging our transcriptomic data, we selected transgenic mouse lines where Cre expression is driven by marker genes that targeted four non-overlapping subgroups of LSNs, enabling us to record and analyze their electrophysiological properties. We found that the firing patterns of the neurons generally fell into two groups: regular-spiking cells, which included *Foxp2* (LSN-1), *Esr1* (LSN-5), and laterally located *Ndnf* neurons (LSN-4); and irregular-spiking cells, which comprised *Lhx2* (LSN-8 and LSN-11) and medially located *Ndnf* neurons (LSN-6). The majority of LSNs are non-adapting regular spiking cells that likely encode continuous signals that are relayed from the hippocampus (Wirtshafter and Wilson, 2021). This is especially true for regular-spiking cells located dorsally, where contextual information about locomotion and spatial navigation is encoded. (Bender et al., 2015; Besnard et al., 2019; Bzymek and Kloosterman, 2023; Chee et al., 2015; Wirtshafter and Wilson, 2020).

The firing pattern of irregular spiking neurons varied: *Lhx2* neurons exhibited transient spiking, likely stemming from their expression of the calcium-dependent potassium channel *Kcnn3* (Sivaramakrishnan and Oliver, 2001), while medial *Ndnf* neurons showed a combination of regular spiking and plateau potentials. The latter could be attributed to voltage-gated calcium channels or persistently active sodium channels, although the specific channels involved are yet to be determined (Teka et al., 2011). The unique firing patterns of those two subgroups suggest that the neurons have specialized functional roles and are only activated by specific contextual information. This notion is supported by the fact that both populations primarily project to areas that are key regulators of motivation and attention—the lateral hypothalamus and the nucleus of the diagonal band, respectively—as well as threat response behaviors (the anterior hypothalamic area). Additionally, all irregular spiking cells displayed short stubby spines, a trait typically observed in neurons that have unique functions (Hayashi and Majewska, 2005; Pchitskaya and Bezprozvanny, 2020). This diversity of action potential waveforms underscores the specialized roles that transcriptionally distinct LSNs have in integrating and processing information across limbic circuits.

Our work provides a detailed description of the projection patterns and presynaptic inputs of genetically distinct subgroups. The hippocampus was the largest source of presynaptic inputs onto LSNs, while the hypothalamus was the main projection target, as reported by others (Albert et al., 1978; Gergues et al., 2020; Raisman, 1969; Risold and Swanson, 1997). However, our data shows that the distribution of these connections vary in a cell type specific manner. Of the groups we studied, *Ndnf* neurons were the only subgroup to predominantly receive innervation from the dorsal hippocampus, and primarily targeted the LHA and NDB. This same connection pattern was described for dorsolateral Somatostatin (*Sst)* expressing LSNs (Besnard et al., 2019), likely corresponding to LSN-4a. Given that *Ndnf* is expressed by

both LSN-6 and LSN-4, we were unable to differentiate between their connections. However, the observation that a subset of LSN-4 shares the same projection pattern with the broader *Ndnf* expressing population suggests that LSN-4 and LSN-6 might have similar synaptic connections.

An intriguing possibility is that LSN-4 and LSN-6 project to the same gross anatomical regions but form connections with different neuronal types. This may also apply to LSN-1 and LSN-9, two subtypes located in adjacent domains within the rostral lateral septum. *Foxp2* expressing LSN-1 is primarily composed of small-bodied cells that receive inputs from the ventral hippocampus and preferentially innervate the medial preoptic area (MPO), a projection pattern similar to that of *Nts* expressing neurons (Azevedo et al., 2020; Chen et al., 2022; Li et al., 2023). Our MERFISH data revealed that both LSN-1 and LSN-9 neurons express *Nts*, considering the established roles of Nts neurons in regulating feeding behaviors, it is likely that both subtypes play significant roles in regulating energy balance. Using, the data presented in this study more targeted genetic tools can be developed to dissect the circuitry of individual LSN subtypes with greater precision.

The identity and function of neurons in the LS are shaped by intrinsic lineage programs and are further defined by extrinsic factors that specify each subtype. Although a comprehensive conceptual model of LS function is yet to be established, our data supports the notion that heterogeneous subtypes of LSNs operate collectively as functional units to regulate distinct physiological, emotional and motivational processes (Besnard and Leroy, 2022). The data we present here lays the groundwork for further dissection of LS functional circuits, offering deeper insights into their roles in regulating different behaviors and aiding our understanding of disease and healthy states controlled the limbic system.

KEY RESOURCES TABLE

REAGEGENT or RESEOURCE	SOURCE	IDENTIFIER
Antibodies		
Mouse monoclonal anti-Nkx2.1	Santa Cruz	53136
Rabbit polyclonal anti-Zic	Segal Lab	N/A
Rabbit monoclonal anti-RFP	Rockland	600-401-379
Chicken polyclonal anti-GFP	Aves	GFP-10020
Chicken polyclonal anti-RFP	Rockland	600-901-379
Goat polyclonal anti-chicken 488	Thermo Fisher	A11039
Goat polyclonal anti-chicken 546	Thermo Fisher	A11040
Goat polyclonal anti-rabbit 488	Thermo Fisher	A11034
Goat polyclonal anti-rabbit 546	Thermo Fisher	A11035
Commercial Assays		

Chromium next GEM single cell 3' v3	10X Genomics	CG000315
MERSCOPE	Vizgen	91600001
RNAscope Fluorescent Multiplex Assay V2	ACD	320513/320293
Experiments models: Organisms/Strains		
Nkx2.1-Cre	Jackson Lab	RRID: IMSR_JAX:008661
NDNF-ires-Cre	Jackson Lab	RRID: IMSR_JAX:030757
Foxp2-ires-Cre	Jackson Lab	RRID: IMSR_JAX:030541
Esr1-Cre	Jackson Lab	RRID: IMSR_JAX:017911
ChAT-IRES-Cre::Δneo	Jackson Lab	RRID: IMSR_JAX:031661
Ai14 (RCL-tdT)-D	Jackson Lab	RRID: IMSR_JAX:007914
CAG-Sun1/sfGFP	Jackson Lab	RRID: IMSR_JAX:030952
Lhx2-CreER	Huang Lab	N/A
Bacterial and virus strains		
mGFP-2A-Synaptophysin-mRuby	Addgene	71760-AAV1
pAAV-CAG-DIO-N2c-2G-P2A-TVA-eGFP	Fishell Lab	N/A
EnvA-CVS-N2c(DG)-mCherry	NIH CNNV core	N/A

LEAD CONTACT AND MATERAL AVAILABILITY

No new reagents were produced from this study. Further information and requests for resources and reagents should be directed to and will be fulfilled by the lead contact,

Corey Harwell (corey.harwell@ucsf.edu)

EXPERIMENTAL MODEL AND STUDY PARTICIPANT DETAILS

Animals

All animal procedures were reviewed and approved by the Institutional Animal Care and Use Committee (IACUC) at both Harvard University and the University of California, San Francisco. The welfare and care of the animals, as well as the conduct of the experiments, strictly adhered to the NIH guidelines. The present study was conducted utilizing both male and female adult mice of C57Bl6/J genetic background, with ages ranging between 30 and 90 days. Animal housing conditions adhered to a 12-hour light/dark cycle, with food and water supplied ad libitum.

METHOD DETAILS

Immunofluorescence

Adult animals were anesthetized with 2.5% Avertin, and were transcardially perfused with PBS, followed by 4% PFA in PBS. Subsequently, their brains were dissected out and subjected to post-fixation in 4% PFA at 4°C overnight. Brain tissues were then sectioned into slices of 75–100 µm thickness using a vibratome (Leica Microsystems VT12000S) and preserved in a freezing buffer (70 g sucrose, 75 ml ethylene glycol, filled to 250 ml with 0.1 sodium phosphate buffer) at -20°C. Before further processing, the sections underwent a washing cycle, consisting of three 5-minute washes in PBS. The sections were then permeabilized in a solution of 10% serum and 0.3% Triton in PBS for one hour. The primary antibodies were diluted in the same solution at concentrations ranging between 1:500-1:1000, and the sections were incubated in this for 24 hours at 4°C. Following another round of washing, as performed previously, the sections were incubated in secondary antibodies, which were diluted in 10% serum in PBS at a concentration of 1:1000. This incubation step lasted for 2 hours at room temperature. After one final wash, the sections were labeled with DAPI (4',6-diamidino-phenylindole, Invitrogen) and subsequently mounted onto a glass slide and cover-slipped using an antifade mounting medium.

Single-nucleus RNA-sequencing and library preparation

A total of six mice (3 male and 3 female) across three replicates were used for this study. Nkx2.1-Cre mice crossed with the conditional Sun1GFP allele were 35 days old at the time of sacrifice. The brain tissue was carefully extracted, and the septum was selectively dissected and immersed in a hibernation buffer consisting of 0.25M sucrose, 25mM KCl, 5mM MgCl2, and 20mM Tricine KOH. Following this, the dissected tissue was gently transferred into a pre-chilled 2 ml Dounce homogenizer containing 500 µl of hibernation buffer supplemented with 5% IGEPAL, half a Roche protease inhibitor tablet, 0.2 U/µl Promega RNasin, 0.1% spermidine, 0.1% DTT, and 0.1% spermine. The tissue was delicately homogenized using loose and tight pestles, approximately 15 strokes each. After a resting period of 10 minutes, the homogenate was transferred to a low-bind Eppendorf tube and centrifuged for 5 minutes at 500 g at 4 °C. The supernatant was discarded, and the pellet was carefully resuspended in 500 µl of 1% BSA in PBS supplemented with 0.2 U/µl Promega RNasin, 0.1% spermidine, 0.1% DTT, and 0.1% spermine. The suspension was centrifuged once again under similar conditions, and the pellet was resuspended as previously outlined. The final suspension was strained through a 40 µm Flowmi filter and stained with 0.8 µl of Ruby Dye prior to Fluorescence-activated Cell Sorting (FACS). Nuclei double positive for GFP and Ruby Dye were separated from nuclei only positive Ruby dye using a SONY SH800S FAC sorter. After collecting a minimum of 50,000 events, the nuclei were loaded onto a 10X Chromium Single Cell 3' chip (v3 chemistry) at the specified concentration. This was followed by adherence to the standard 10X Chromium Single Cell 3' protocols (v3 chemistry). Finally, the resultant libraries were sequenced using a NovaSeq 6000 S4 flow cell, achieving a read depth of approximately 50,000 reads per nucleus.

Single nuclei-sequencing analysis

The sequenced reads were aligned to the mouse genome (mm10), inclusive of intronic reads, using the Cellranger 7.1.0 software package from 10X Genomics. The mean numbers of UMIs and genes per cell were noted as 3,287 and 3,014 respectively. For the subsequent analysis, we utilized the Python module Scanpy (Wolf et al., 2018). The raw count matrix of each sample was loaded into a AnnData file, and all samples were concatenated into one AnnData file. Genes expressed in less than 3 cells were filtered out, along with cells that expressed fewer than 200 genes.

We then normalized the raw counts to 10,000 reads per cell before identifying the highly variable genes. Following this process, we performed principal component (PC) analysis and computed the PC variance ratio to determine how much each PC contributed to the total variance. From this, we determined that the first 15 PCs were sufficient to explain the total variance and were used to construct a neighborhood graph of our cells. Subsequently, this graph was embedded in two-dimensions for visualization using unifold manifold approximation and projection (UMAP) dimensionality reduction. Batch effect between replicates was corrected for using BBKNN (Polański et al., 2020). We then performed Leiden clustering at multiple resolutions to understand how the clusters evolved as a function of resolution. Using a resolution of 0.9 we performed pairwise differential gene analysis between the clusters and all other cells using the Wilcoxon rank-sum test. Our general cell types were annotated by cross-referencing established marker genes or evaluating the regionalization of genes enriched in our clusters that were accessible via the Allen Brain *in situ* hydrization resource (Lein et al., 2007). Once general cell types were established, we subclustered the LS neurons and performed the same dimensionality reduction, embedding, and marker gene analysis mentioned previously.

SCENIC Regulon analysis

Regulon analysis was performed using the pySCENIC Python implimintation of the SCENIC pipeline (Aibar et al., 2017). The raw count matrix for LS neurons was used to ‘infer regulons (transcription factors and their targets) based on correlations of gene expression across cells using the arboreto package, which utilizes GRNBoost2 (Moerman et al., 2019). Target genes that had no enrichment for the transcription factor binding motif within a genome search space between 500 bp and 10kb around the transcriptions start site were then pruned. Subsequently, the ‘aucell’ package was used to compute an area under curve value for each regulon across all cells. Finally, regulon specificity scores were computed for both GFP-positive and -negative LS neurons to determine which regulons were enriched in either population.

Gene ontology enrichment

We employed the 'ClusterProfiler' R package to conduct gene ontology (GO) analysis on GFP-positive and -negative LS neurons (Wu et al., 2021; Yu, 2020). Initially, differentially expressed genes between these two types of neurons were identified. Genes co-expressed in clusters with a majority of GFP-positive or -negative cells were then selected. The resultant gene list was subjected to a hypergeometric test to pinpoint overrepresented GO terms, categorized under three domains: biological process, cellular component, and molecular function. The same process was applied to the list of spatially variable genes. Terms with a p-value below 0.05 were deemed significantly enriched.

Selection of MERFISH Gene Panel

A multi-pronged approach was used to curate a 500 gene MERFISH panel, aiming to identify the same transcriptionally distinct cell types found in the single-nucleus RNA-seq dataset. We began by manually incorporating genes recognized as well-established general cell type markers. Subsequently, used the single-nucleus sequencing dataset as reference to identify genes showing enrichment in each of our cell types of interest. This was accomplished by performing pairwise differential gene expression analysis between cell groups. Finally, we employed the random forest classifier scRFE on the single-nucleus dataset to identify the sets of genes that best describe our cell groups (Park et al., 2020). This list was uploaded and approved for probe encoding by the Vizgen Gene Panel Design Portal.

MERFISH sample preparation and hybridization

We utilized 35-day-old C57Bl6/J mice, both male and female, in our study. Following anesthesia with 2.5% Avertin, the animals were scarified and their brain tissues were carefully extracted. The harvested tissues were immediately preserved in OCT (Optimal Cutting Temperature compound) and uniformly frozen using dry ice. Subsequently, the tissues were stored at -80°C for future use. 24 hours prior to sectioning, the samples were warmed to -20°C, after which serial cryosectioning was conducted at a thickness of 10 micrometers. Several coronal sections, representing different areas of the LS along the rostral-caudal axis, were mounted onto a glass slide from the Vizgen MERSCOPE Slide Box. The mounted sections were fixed with 4% PFA in 1X PBS, rinsed, permeabilized, and preserved in sterile 70% ethanol. The procedures of probe hybridization, gel-embedding, and tissue clearing were performed according to the MERSCOPE sample preparation user guide. Briefly, we washed the sections with a formamide wash buffer (PN 20300003) and incubated them for 30 minutes at 37°C, before the probe hybridization mix was added. The sections were then incubated at 37°C for 48 hours while submerged in the MERFISH library mix. After probe incubation, we washed the sections with formamide buffer two times for 30 minutes each at 47°C, and once with sample prep wash buffer (PN 20300001). We then

applied a gel embedding solution containing 10% ammonium persulfate, tetramethylethylenediamine, and a gel embedding premix (PN 20300004). A cover slip provided by the MERSCOPE Slide Box was used to slowly spread the gel embedding solution over the sections, and the gel was solidified at room temperature for 1.5 hours. Once solidified the coverslip was slowly removed, and a clearing solution containing Warm Clearing Premix (PN 20300003) and proteinase K was incubated with the sections at 37°C for 24 hours.

MERFISH image analysis and cell segmentation

After gel clearing, the samples were rinsed with the Wash Buffer provided in the Vizgen Imaging Kit and then placed into the MERSCOPE instrument flow cell. After the assembly of fluidics and requisite reagents, a low-resolution image of DAPI signal was captured using a 10X objective lens in a tilescan format. Areas exhibiting well-preserved lateral septal samples were delineated as regions of interest. Following the marking of all such regions, multiple rounds of 3-color imaging were conducted using a 60X objective lens. During each imaging round, seven focal planes along the z-axis were captured for each channel. The raw image files obtained were processed via the MERlin image analysis pipeline (Moffitt et al., 2018). The Cellpose2 software was utilized to segment cells from the nuclear DAPI signal (Pachitariu and Stringer, 2022). The decoded RNA molecules were then partitioned into individual cells to generate single-cell count matrices.

MERFISH Clustering Analysis

The coordinates and count matrix from the MERFISH data were imported as an AnnData object. Cells with a volume larger than 200 um^3, with fewer than 100 transcripts, and with a DAPI score less than 500 were excluded from the analysis. The remaining cells were then subjected to standard single-cell analysis following previously described protocols.

Spatially variable gene patterns

Spatially variable genes were ascertained from our MERFISH data utilizing SpatialDE (Svensson et al., 2018). This analysis allowed us to model gene expression levels in relation to the spatial coordinates of cells and assign rankings to genes based on the degree of spatial variability in their expression. Following this, automatic expression histology was employed to recognize genes exhibiting similar patterns of expression across the tissue. This methodology was applied to five representative sections. By manually matching patterns across these sections and annotating them based on their expression throughout the lateral septum, we were able to generate a detailed map of spatially variable gene expression.

Stereotaxic Viral Injections

All surgical procedures were executed under aseptic conditions. Mice aged 2-6 months were anesthetized with isoflurane, followed by an injection of either 1.5 mg/kg SR Buprenorphine or 3.25 mg/kg EthicaXR, in addition to a 5 mg/kg dose of Meloxicam. They were then placed on a heating pad with their head fixed on a stereotaxic apparatus (Kopf). Their eyes were protected from drying using an ophthalmic ointment, and their hair was removed from the scalp to allow for an incision that exposed the cranium. After leveling the skull, a hole was drilled into it at coordinates that targeted the lateral septum: ChATCre: AP +0.49 mm, ML 0.47 mm, DV -3.3 mm; Esr1Cre: AP +0.25 mm, ML 0.5 mm, DV -3.3 mm; NdnfCre: AP +0.13 mm, ML 0.3 mm, DV -2.5 mm; Foxp2Cre: AP +1.09 mm, ML 0.45 mm, DV -3.5 mm. Glass capillaries were backfilled with mineral oil and front-filled virus, before being loading into a Hamilton syringe. Subsequently the syringe was connected to a nanoliter injector (WPI) which delivered our targeted volume of injection at a rate of 25 nl/s. After 10 minutes, the capillary was slowly removed from the brain and the incision was sutured. The mice were allowed to recover partially from anesthesia before being returned to their cage.

For the anterograde tracing experiments, 50-100 nl of pAAV hSyn FLEx mGFP-2A-Synaptophysin-mRuby was injected into the lateral septum of Ndnf-Cre, Esr1-Cre, Chat-Cre, and Foxp2-Cre mice. The monosynaptic rabies tracing experiments required two surgical procedures. First mice were injected with 50-100 nl of a helper virus pAAV-CAG-DIO-N2c-2G-P2A-TVA-eGFP. Three weeks later a second surgery was performed to inject 50 nl of the Rabies EnvA-CVS-N2c(DG)-mCherry virus. The mice were euthanized five days after the second injection, and their brain tissue was collected.

Electrophysiology recordings and cell filling

Adult mice were initially anesthetized with 2.5% Avertin, followed by transcardial perfusion with 5 ml of ice-cold, oxygenated slice solution saturated with 95% O2 and 5% CO2. The slice solution consisted of the following components (in mM): 110 choline chloride, 2.5 KCl, 0.5 CaCl2, 7 MgCl2, 1.3 NaH2PO4, 25 NaHCO3, 10 glucose, 1.3 Na-ascorbate, and 0.6 Na-pyruvate. The osmolarity of the slice solution was adjusted to 305–315 mOsm/L using sucrose. After perfusion, the brains of the mice were extracted and placed in ice-cold, oxygenated slice solution. Using a vibratome (VT1200s, Leica), the brain tissue was carefully sectioned into 200 µm thick slices. These slices were then incubated for at least 1 hour at 33°C in oxygenated artificial cerebrospinal fluid (ACSF) containing (in mM): 125 NaCl, 2.5 KCl, 2 CaCl2, 1.3 MgCl2, 1.3 NaH2PO4, 1.3 Na-ascorbate, 0.6 Na-pyruvate, 10 glucose, and 25 NaHCO3 (305-315 mOsm/L). Following incubation, brain slices were transferred to a recording chamber at room temperature for subsequent recordings.

During the recordings, slices were continuously perfused with ACSF at a flow rate of 3 ml/min. For whole-cell recordings, glass recording pipettes (3–6 MΩ) were prepared using a P-87 glass pipette puller (Sutter Instrument). The pipettes for whole-cell recordings were filled with an internal solution composed of (in mM): 130 K-gluconate, 10 HEPES, 0.6 EGTA, 5 KCl, 3 Na2ATP, 0.3 Na3GTP, 4 MgCl2, and 10 Na2-phosphocreatine, with a pH of 7.2–7.4 and osmolarity of 295–305 mOsm/L.

For neurobiotin microinjection, neurobiotin (2.5 mg/ml; Vector Laboratories, Burlingame, CA, United States) was dissolved in the internal solution. We conducted whole-cell recordings from lateral septum neurons, with the pipette filled with Neurobiotin. After establishing a whole-cell configuration, neurons were held for at least 15 minutes in current clamp and injected with a depolarizing current (500 ms, 500 pA, 1 Hz) to allow for sufficient diffusion of neurobiotin into the cell. At the end of each recording session, the pipette was slowly withdrawn to maintain the cell's integrity, and the slice was immediately fixed in 4% paraformaldehyde in PBS overnight at 4°C. Post-fixation, slices were washed in PBS and then incubated overnight at 4°C in a solution containing Streptavidin-conjugated Alexa Fluor 488 (1:500 in PBS) to visualize neurobiotin-filled neurons. The slices were then rinsed in PBS, mounted onto slides, and cover-slipped using an antifade mounting medium.

Data were collected using a MultiClamp 700B amplifier (Molecular Devices) and ITC-18 A/D board (HEKA) with AxoGraph software. The neurons were held at -65 mV. The traces were low-pass filtered at 3 kHz and digitized at 10 kHz.The electrophysiological data were analyzed using Easy Electrophysiology. The resting membrane potential was recorded immediately after break-in under I=0 mode. The input resistance of the cell was calculated from the peak of the voltage response to a 200pA hyperpolarized current. The sag or hump amplitude was calculated with a 200pA hyperpolarized current injection. Action potentials were counted using the Action Potential Counting module across current steps from -200 to 200 pA. Action potential properties were analyzed using the Action Potential Kinetics module across current steps from -200 to 200 pA. Threshold was defined as the voltage at the point when the slope first exceeded a value of 20 V/s. Rheobase was defined as the amplitude of the depolarized current injections when the first action potential was observed. Spike half-width is defined as the width at half amplitude. Fast after-hyperpolarization (fAHP) is defined as the difference between the action potential threshold and the minimum voltage after the action potential within 3 ms. Medium after-hyperpolarization (mAHP) is calculated as the difference between the action potential threshold and the minimum voltage after the action potential, from 10 to 50 ms.

Quantification and Statistical Analysis

Cell counting was done manually using the CellCounter tool in ImageJ. For the lateral septum, the dorsal, intermediate, and ventral regions were designated according to the historical literature (Alonso and

Frotscher, 1989). All other regions were designated using the Allen brain atlas. The synaptophysin signal was quantified by measuring the fraction of the total area covered by synaptophysin fluorescence across all brain regions. Basic analysis and plotting were performed using GraphPad's Prism software or the matplotlib module in Python.

Microscopy and image analysis

Image acquisition was conducted utilizing a Leica Stellaris 8 confocal microscope, using the 10X, 20X, 40X, and 63X objectives based on the specific requirements of each set of samples. All parameters, such as image acquisition speed, resolution, averaging, zoom, and z-stack, were accordingly adjusted. Post-acquisition, the images were analyzed using the ImageJ software.

Author contributions

Conceptualization, C.M.R. and C.C.H.; Investigation C.M.R., Y.R., Y.X., M.T.G., D.T, S.V., J.L, M.A.A., S.M.H.; Resources, A.O.P., and C.C.H.; Writing, C.M.R. and C.C.H.; Editing, C.M.R., Y.X., M.T.G., Y.R., C.C.H.; Funding Acquisition, C.C.H.; Supervision, C.C.H.

Acknowledgements

We thank members of the Harwell lab for feedback on the manuscript; Sandra Chang for lab infrastructure support. We are grateful to the Gord Fishell for providing the N2c-Rabies helper virus and Josh Huang for providing the Lhx2-CreER line. Lastly, we would like to thank the Single Cell Core at Harvard Medical School, Boston, MA for performing the single cell RNA-Seq sample preparation. This research was supported by NIH Grants R01MH119156 and R01NS102228 to CCH and the HHMI Gilliam Fellowship to C.M.R.

Declaration of interests

The authors declare no competing interests.

Figure Legends

Figure 1: Transcriptional taxonomy of lateral septal neuron subtypes

A. Coronal section of the lateral septum immunofluorescently stained for RFP (magenta) and ZIC (cyan) in a P35 Nkx2.1-Cre animal carrying the Ai14 reporter allele. Scale bar: 100 μm **B.** Bar graphs showing the proportion of NeuN positive cells that are RFP positive (magenta) N = 4. The left graph shows counts

for the dorsal, intermediate, and ventral subregions of the LS. Right graph shows the counts for four regions along the anterior-posterior axis; from Bregma section 1 (S1): +0.9, section 2 (S2): +0.6, section 3 (S3): +0.3, section 4 (S4): 0.0. **C.** Schematic detailing our genetic strategy and single nucleus-sequencing approach. **D.** UMAP plot showing the GFP identity of all 25,173 cells collected (N=6). GFP positive cells (magenta) indicate *Nkx2.1* lineage, while GFP negative cells (cyan) are outside of the *Nkx2.1* lineage **E.** UMAP plot of all cells showing the general cell type annotations. Lateral septal neurons (LSN), Diagonal band neurosn (DbN), medial septal neurons (MSN), striatal neurons (StrN), island of Calleja neurons (IoCN), triangular septal neurons (TSN), medial habenula neurons (MHN), thalamic neurons (ThN), neuroblasts (Nb), lateral septal astrocytes (LSA), medial septal astrocytes (MSA), oligodendrocytes (Oligo), oligodendrocyte precursor cells (OPC), microglia (Micro). **F.** UMAP plot showing the GFP identity of 5,103 LSNs. **G)** UMAP plot of transcriptionally distinct LSN subtypes. **H.** Feature plots showing the scaled expression (scale bar) of marker genes uniquely enriched in LSN subtypes. **I.** Dot plot showing the scaled average gene expression (scale bar) of the minimal markers necessary to define each LSN subtype. **J.** Heatmap showing the top 10 differentially enriched genes for each LSN subtype. **K.** Stacked bar graph shoFwing the proportion GFP positive (magenta) or negative (cyan) cells in each LSN subtype. Dendrogram based on hierarchical clustering analysis using the average total gene expression of each LSN subtype.

Figure 2: Molecular features of developmentally distinct lateral septal neurons

A. Volcano plot showing 687 differentially expressed genes between Nkx2.1+ (magenta) and Nkx2.1- (cyan) LSNs. **B.** Feature plot showing the scaled expression (scale bar) patterns of *Sfta3-ps, Meis2,* and *Nkx2.1* among LSNs*,* compared with a UMAP plot of their GFP identity. **C.** Violin plots showing the scaled expression of *Sfta3-ps* and *Meis2* across the LSN subtypes. On top is a stacked bar graph showing the proportion of GFP positive (magenta) and negative (cyan) cells in each LSN subtype. **D.** Feature plots showing the module score enrichment (scale bar) of inferred target genes for NKX2.1 and RARB. **E.** Dot plot showing the scaled average gene expression (scale bar) of the top 20 differentially expressed genes between Nkx2.1+ (magenta) and Nkx2.1- (cyan) LSNs. Red asterisks mark genes that were predicted to be regulated by NKX2.1 or RARB in Nkx2.1+ and Nkx2.1- neurons respectively. On top is a stacked bar graph showing the proportion of GFP positive (magenta) and negative (cyan) cells in each LSN subtype. Subtypes are arranged by their proportion of GFP positive cells from lowest to highest. **F.** Gene-concept plot constructed from gene ontology analysis of the top 50 differentially enriched genes between Nkx2.1+ (magenta) and Nkx2.1- (cyan) LSNs. Genes are linked to their associated molecular function term, with the size of colored nodes representing the number of linked genes.

Figure 3: Anatomical organization of lateral septal neuron subtypes

A. Schematic detailing the processing of MERFISH samples. **B.** UMAP plot of 44,715 LSNs segmented from the MERFISH dataset (N=2), annotated to show LSN subtypes. **C.** Heatmap showing the Pearson's correlation between the MERFISH and snRNA-seq LSN clusters using their scaled average total gene expression (scale bar). **D.** Spatial plot showing the distribution of LSN subtypes in the MERFISH dataset across 5 representative coronal sections along the anterior-posterior axis: +1.2, +0.9, +0.6, +0.3, +0.0. On top in red are the minimal marker genes necessary to identify each group. **E.** UMAP plot of LSNs in the MERFISH dataset showing the secondary separation of LSN subtypes. **F.** Pie chart showing the percentage of total LSNs for each subtype in the MERFISH dataset. **G.** Spatial plot showing the anatomical distribution of the secondary subtypes for LSN-4, 6, and 7. On top in green are the additional markers needed to distinguish the secondary groups. **H.** Dot plot showing the scaled average expression (scale bar) of genes enriched across the higher resolution subtypes.

Figure 4: Spatially variable genes define the taxonomy of lateral septal neuron subtypes

A. Feature plots showing the scaled module score enrichment (scale bar) for 8 gene-sets that contain spatially variable genes. **B.** Spatial plots showing the anatomical expression pattern for each spatially variable gene-set across 5 coronal sections of the LS. **C.** Dot plot showing the scaled average module score enrichment (scale bar) for each spatially variable gene-set. On top is a stacked bar graph showing the proportion of GFP positive (magenta) or negative (cyan) cells in each LSN subtype, along with a dendrogram constructed from hierarchal clustering analysis using the average total gene expression of each LSN subtype. Dots highlighted in red are the three pairs of developmentally distinct subtypes: LSN 1 and 3, 6 and 8, 5 and 12. **D.** Bar plot constructed from gene ontology analysis showing the number of spatially variable genes associated with a given molecular function. The scale bar shows the adjusted p-value for each molecular function. **E.** Heatmap showing the scaled expression (scale bar) of spatially variable genes grouped according to their general function. On top is a dendrogram constructed from hierarchal clustering analysis using the average total gene expression of each LSN subtype. Red borders highlight the values for three pairs of developmentally distinct subtypes: LSN 1 and 3, 6 and 8, 5 and 12.

Figure 5: Electrophysiological and morphological properties of lateral septal neuron subgroups

A. Feature plot showing the scaled expression (scale bar) of four genes that mark non-overlapping subgroups of LSNs. **B.** Dot plot showing the scaled average expression of four genes that mark non-overlapping subgroups of LSNs. On top is a stacked bar graph showing the proportion of GFP positive (magenta) or negative (cyan) cells in each LSN subtype, along with a dendrogram constructed from hierarchal clustering analysis using the average total gene expression of each LSN subtype. **C.** Spatial plot showing the anatomical positioning of four genetically distinct LSN subgroups across 5 coronal sections of the LS. **D.** Morphological traces from neurobiotin filled LSNs for each genetically defined

group. **E.** High magnification images of neurobiotin filled (Esr1, Ndnf-Lateral, Ndnf-Medial, and Foxp2) or tdTomato fluorescent (Lhx2) cells for each genetically defined group. The top row shows their somas, and bottom bar shows their dendrites (scale bars 10 μm). **F.** Representative traces showing the firing pattern of cells recorded using voltage clamp from each genetically defined LSN subgroup. Current was injected in 25pA steps ranging from -200 to 150pA, with higher currents shaded in darker colors. **G.** Phase plot showing the membrane voltage rate change for a representative action potential for a 100pA current injection for each LSN subgroup. **H.** Heatmap showing the scaled values (scale bar) for 14 intrinsic properties. On top is a dendrogram showing the relationships among subgroups based on the intrinsic properties**. I**. Heatmap showing the scaled average expression (scale bar) of voltage gated ion channels that are differentially expressed among LSNs. The genes are organized in accordance with their ion channel family.

Figure 6: Anatomical connections of lateral septal neurons subgroups

A. Schematic showing a local injection of an AVV expressing a Cre dependent eGFP and synaptophysin fused RFP into the LS of four transgenic. **B.** Representative images for each transgenic line showing coronal sections of the LS immunofluorescently stained for GFP after a local AAV. Scale bar: 100 μm. **C.** Bar graph illustrating the regional proportion of total synaptophysin fluorescence for each Cre line: Chat-Cre (N = 4), Esr1-Cre (N=3), Ndnf-Cre (N=4), Foxp2-Cre (N=2). **D.** Representative images showing GFP-expressing projections of LSN subgroups labeled in each Cre line. Scale bar: 100 μm **E.** Schematic showing a helper AAV expressing a Cre-dependent eGFP, TVA, and N2c-G protein, along with the Rabies-N2c virus being injected into the LS of each transgenic line. **F.** Bar graph illustrating the regional proportion of total labeled cells for each rabies injected Cre line: Chat-Cre (N = 3), Esr1-Cre (N=2), Ndnf-Cre (N=4), Foxp2-Cre (N=2) **G.** Heatmap showing the fraction of rabies labeled cells across nine regions for each transgenic line: hippocampus (hippo), hypothalamus (Hypo), lateral septum (LS), amygdala (Amy), cerebral cortex (Cortex), subpallium (Subpal), thalamus (Thal), olfactory regions (Olfactory), and midbrain nuclei/ brain stem (MB/BS). **H.** Representative images showing differences in retrograde labeling in the dorsal and ventral CA1/CA3 regions of the hippocampus, along with several subregions of the hypothalamus: medial preoptic nucleus (MPN), posterior hypothalamus (PH), ventral premammillary nucleus (PMv), posterior periventricular hypothalamus (PVp), and ventral tubular mammillary nucleus (TMv). **I.** Representative images showing differences in retrograde labeling within the lateral septal nuclei for each transgenic line.

Figure S1: Distribution of *Nkx2.1* lineage cells in the lateral septum

A. Coronal sections of the lateral septum across four representative sections along the anterior-posterior axis (AP position from Bregma, from left to right: 0.9, 0.6, 0.3, 0.0) immunofluorescently stained for RFP (magenta) and ZIC (cyan) in a P35 Nkx2.1-Cre animal carrying the Ai14 reporter allele. Scale bar: 100 μm. B. Bar graphs showing the proportion of NeuN and RFP positive cells that are ZIC positive, N = 4. The left graph shows counts for the dorsal, intermediate, and ventral subregions of the LS. Right graph shows the counts for the same four regions along the anterior-posterior axis as Figure 1.

Figure S2: Single-nucleus RNA-seq molecular classification of cell types in the septum

A. UMAP plots showing Leiden clusters for all cells at four different resolutions. **B.** Feature plot showing the scaled expression of genes used to identify our major cell groups. **C.** Stacked bar graph showing the proportion of GFP positive (magenta) and negative (cyan) cells for each major group. **D.** UMAP plots showing Leiden clusters for LSNs at three different resolutions.

Figure S3: Lineage specific gene regulatory networks in lateral septal neurons

A. Regulon specificity score for GFP positive and negative LSNs. The top five enriched regulons are highlighted in red.

Figure S4: Shared transcriptomic features between developmentally distinct lateral septal neurons

A. Heatmap showing the top 20 differentially expressed genes for each developmentally distinct paired group, against all other LSNs. **B.** Feature plot showing the pattern of scaled gene expression pattern among LSNs for genes specifically enriched in the developmentally distinct pairs.

Figure S5: Identification of lateral septal neurons using MERFISH

A. UMAP plot showing Leiden clusters at several resolutions for 263,947 cells collected using MERFISH. **B.** Feature plot showing the scaled gene expression of pattern among LSNs for genes specifically enriched in lateral septal neurons.

Figure S6: Classification of spatially variable genes in the lateral septum

A. Heatmap plot showing the neighborhood enrichment values for each LSN subtype **B.** Spatial plot showing the positioning of developmentally distinct LSN subtype pairs. **C.** Spatial plots showing the automatic expression histology of spatially variable genes across 5 coronal sections of the LS.

REFERENCES

Agoston, Z., Heine, P., Brill, M.S., Grebbin, B.M., Hau, A.-C., Kallenborn-Gerhardt, W., Schramm, J., Götz, M., Schulte, D., 2014. Meis2 is a Pax6 co-factor in neurogenesis and dopaminergic periglomerular fate specification in the adult olfactory bulb. Development 141, 28–38. https://doi.org/10.1242/dev.097295

Aibar, S., González-Blas, C.B., Moerman, T., Huynh-Thu, V.A., Imrichova, H., Hulselmans, G., Rambow, F., Marine, J.-C., Geurts, P., Aerts, J., van den Oord, J., Atak, Z.K., Wouters, J., Aerts, S., 2017. SCENIC: single-cell regulatory network inference and clustering. Nat. Methods 14, 1083–1086. https://doi.org/10.1038/nmeth.4463

Albert, D.J., Brayley, K.N., Milner, J.A., 1978. Connections from the lateral septum modulating reactivity in the rat. Physiol. Behav. 21, 761–767. https://doi.org/10.1016/0031-9384(78)90016-1

Alonso, J.R., Frotscher, M., 1989. Organization of the septal region in the rat brain: A Golgi/EM study of lateral septal neurons. J. Comp. Neurol. 286, 472–487. https://doi.org/10.1002/cne.902860406

Alvarez-Buylla, A., 1997. Mechanism of migration of olfactory bulb interneurons. Semin. Cell Dev. Biol. 8, 207–213. https://doi.org/10.1006/scdb.1996.0134

An, M., Kim, H.-K., Park, H., Kim, K., Heo, G., Park, H.-E., Chung, C., Kim, S.-Y., 2022. Lateral Septum Somatostatin Neurons are Activated by Diverse Stressors. Exp. Neurobiol. 31, 376–389. https://doi.org/10.5607/en22024

Anthony, T.E., Dee, N., Bernard, A., Lerchner, W., Heintz, N., Anderson, D.J., 2014. Control of Stress-Induced Persistent Anxiety by an Extra-Amygdala Septohypothalamic Circuit. Cell 156, 522–536. https://doi.org/10.1016/j.cell.2013.12.040

Azevedo, E.P., Tan, B., Pomeranz, L.E., Ivan, V., Fetcho, R., Schneeberger, M., Doerig, K.R., Liston, C., Friedman, J.M., Stern, S.A., 2020. A limbic circuit selectively links active escape to food suppression. eLife 9, e58894. https://doi.org/10.7554/eLife.58894

Azzarelli, R., Hardwick, L.J.A., Philpott, A., 2015. Emergence of neuronal diversity from patterning of telencephalic progenitors. WIREs Dev. Biol. 4, 197–214. https://doi.org/10.1002/wdev.174

Ba-Charvet, K.T.N., Brose, K., Marillat, V., Kidd, T., Goodman, C.S., Tessier-Lavigne, M., Sotelo, C., Chédotal, A., 1999. Slit2-Mediated Chemorepulsion and Collapse of Developing Forebrain Axons. Neuron 22, 463–473. https://doi.org/10.1016/S0896-6273(00)80702-3

Bagri, A., Marín, O., Plump, A.S., Mak, J., Pleasure, S.J., Rubenstein, J.L.R., Tessier-Lavigne, M., 2002. Slit Proteins Prevent Midline Crossing and Determine the Dorsoventral Position of Major Axonal Pathways in the Mammalian Forebrain. Neuron 33, 233–248. https://doi.org/10.1016/S0896-6273(02)00561-5

Bandler, R.C., Vitali, I., Delgado, R.N., Ho, M.C., Dvoretskova, E., Ibarra Molinas, J.S., Frazel, P.W., Mohammadkhani, M., Machold, R., Maedler, S., Liddelow, S.A., Nowakowski, T.J., Fishell, G., Mayer, C., 2022. Single-cell delineation of lineage and genetic identity in the mouse brain. Nature 601, 404–409. https://doi.org/10.1038/s41586-021-04237-0

Bean, B.P., 2007. The action potential in mammalian central neurons. Nat. Rev. Neurosci. 8, 451–465. https://doi.org/10.1038/nrn2148

Bender, F., Gorbati, M., Cadavieco, M.C., Denisova, N., Gao, X., Holman, C., Korotkova, T., Ponomarenko, A., 2015. Theta oscillations regulate the speed of locomotion via a hippocampus to lateral septum pathway. Nat. Commun. 6, 8521. https://doi.org/10.1038/ncomms9521

Besnard, A., Gao, Y., TaeWoo Kim, M., Twarkowski, H., Reed, A.K., Langberg, T., Feng, W., Xu, X., Saur, D., Zweifel, L.S., Davison, I., Sahay, A., 2019. Dorsolateral septum somatostatin interneurons gate mobility to calibrate context-specific behavioral fear responses. Nat. Neurosci. 22, 436–446. https://doi.org/10.1038/s41593-018-0330-y

Besnard, A., Leroy, F., 2022. Top-down regulation of motivated behaviors via lateral septum sub-circuits. Mol. Psychiatry 27, 3119–3128. https://doi.org/10.1038/s41380-022-01599-3

Blockus, H., Rolotti, S.V., Szoboszlay, M., Peze-Heidsieck, E., Ming, T., Schroeder, A., Apostolo, N., Vennekens, K.M., Katsamba, P.S., Bahna, F., Mannepalli, S., Ahlsen, G., Honig, B., Shapiro, L., de Wit, J., Losonczy, A., Polleux, F., 2021. Synaptogenic activity of the axon guidance molecule Robo2 underlies hippocampal circuit function. Cell Rep. 37, 109828. https://doi.org/10.1016/j.celrep.2021.109828

Bobola, N., Sagerström, C.G., 2024. TALE transcription factors: Cofactors no more. Semin. Cell Dev. Biol., Hox genes: The Original Body Builders 152–153, 76–84. https://doi.org/10.1016/j.semcdb.2022.11.015

Burke, K.J., Bender, K.J., 2019. Modulation of Ion Channels in the Axon: Mechanisms and Function. Front. Cell. Neurosci. 13.

Bzymek, K., Kloosterman, F., 2023. Theta cycle dynamics of spatial representations in the lateral septum. eLife 12. https://doi.org/10.7554/eLife.90207.1

Catani, M., Dell'Acqua, F., Thiebaut de Schotten, M., 2013. A revised limbic system model for memory, emotion and behaviour. Neurosci. Biobehav. Rev. 37, 1724–1737. https://doi.org/10.1016/j.neubiorev.2013.07.001

Cembrowski, M.S., Wang, L., Sugino, K., Shields, B.C., Spruston, N., 2016. Hipposeq: a comprehensive RNA-seq database of gene expression in hippocampal principal neurons. eLife 5, e14997. https://doi.org/10.7554/eLife.14997

Challis, R.C., Ravindra Kumar, S., Chan, K.Y., Challis, C., Beadle, K., Jang, M.J., Kim, H.M., Rajendran, P.S., Tompkins, J.D., Shivkumar, K., Deverman, B.E., Gradinaru, V., 2019. Systemic AAV vectors for widespread and targeted gene delivery in rodents. Nat. Protoc. 14, 379–414. https://doi.org/10.1038/s41596-018-0097-3

Chee, S.-S.A., Menard, J.L., Dringenberg, H.C., 2015. The lateral septum as a regulator of hippocampal theta oscillations and defensive behavior in rats. J. Neurophysiol. 113, 1831–1841. https://doi.org/10.1152/jn.00806.2014

Chen, Z., Chen, G., Zhong, J., Jiang, S., Lai, S., Xu, H., Deng, X., Li, F., Lu, S., Zhou, K., Li, C., Liu, Z., Zhang, X., Zhu, Y., 2022. A circuit from lateral septum neurotensin neurons to tuberal nucleus controls hedonic feeding. Mol. Psychiatry 27, 4843–4860. https://doi.org/10.1038/s41380-022-01742-0

Creps, E.S., 1974. Time of neuron origin in preoptic and septal areas of the mouse: An autoradiographic study. J. Comp. Neurol. 157, 161–243. https://doi.org/10.1002/cne.901570205

Delgado, R.N., Allen, D.E., Keefe, M.G., Mancia Leon, W.R., Ziffra, R.S., Crouch, E.E., Alvarez-Buylla, A., Nowakowski, T.J., 2022. Individual human cortical progenitors can produce excitatory and inhibitory neurons. Nature 601, 397–403. https://doi.org/10.1038/s41586-021-04230-7

Dulac, C., O'Connell, L.A., Wu, Z., 2014. Neural control of maternal and paternal behaviors. Science 345, 765–770. https://doi.org/10.1126/science.1253291

Dupacova, N., Antosova, B., Paces, J., Kozmik, Z., 2021. Meis homeobox genes control progenitor competence in the retina. Proc. Natl. Acad. Sci. 118, e2013136118. https://doi.org/10.1073/pnas.2013136118

Elias, L.A.B., Potter, G.B., Kriegstein, A.R., 2008. A Time and a Place for Nkx2-1 in Interneuron Specification and Migration. Neuron 59, 679–682. https://doi.org/10.1016/j.neuron.2008.08.017

Flames, N., Pla, R., Gelman, D.M., Rubenstein, J.L.R., Puelles, L., Marín, O., 2007. Delineation of Multiple Subpallial Progenitor Domains by the Combinatorial Expression of Transcriptional Codes. J. Neurosci. 27, 9682–9695. https://doi.org/10.1523/JNEUROSCI.2750-07.2007

Fouquet, C., Meglio, T.D., Ma, L., Kawasaki, T., Long, H., Hirata, T., Tessier-Lavigne, M., Chédotal, A., Nguyen-Ba-Charvet, K.T., 2007. Robo1 and Robo2 Control the Development of the Lateral Olfactory Tract. J. Neurosci. 27, 3037–3045. https://doi.org/10.1523/JNEUROSCI.0172-07.2007

Gallagher, J.P., Zheng, F., Hasuo, H., Shinnick-Gallagher, P., 1995a. Activities of neurons within the rat dorsolateral septal nucleus (DLSN). Prog. Neurobiol. 45, 373–395. https://doi.org/10.1016/0301-0082(95)98600-A

Gallagher, J.P., Zheng, F., Hasuo, H., Shinnick-Gallagher, P., 1995b. Activities of neurons within the rat dorsolateral septal nucleus (DLSN). Prog. Neurobiol. 45, 373–395. https://doi.org/10.1016/0301-0082(95)98600-A

Gaston-Massuet, C., Henderson, D.J., Greene, N.D.E., Copp, A.J., 2005. Zic4, a zinc-finger transcription factor, is expressed in the developing mouse nervous system. Dev. Dyn. 233, 1110–1115. https://doi.org/10.1002/dvdy.20417

Gergues, M.M., Han, K.J., Choi, H.S., Brown, B., Clausing, K.J., Turner, V.S., Vainchtein, I.D., Molofsky, A.V., Kheirbek, M.A., 2020. Circuit and molecular architecture of a ventral hippocampal network. Nat. Neurosci. 23, 1444–1452. https://doi.org/10.1038/s41593-020-0705-8

Glerup, S., Bolcho, U., Mølgaard, S., Bøggild, S., Vaegter, C.B., Smith, A.H., Nieto-Gonzalez, J.L., Ovesen, P.L., Pedersen, L.F., Fjorback, A.N., Kjolby, M., Login, H., Holm, M.M., Andersen, O.M., Nyengaard, J.R., Willnow, T.E., Jensen, K., Nykjaer, A., 2016. SorCS2 is required for BDNF-dependent plasticity in the hippocampus. Mol. Psychiatry 21, 1740–1751. https://doi.org/10.1038/mp.2016.108

Gonda, Y., Namba, T., Hanashima, C., 2020. Beyond Axon Guidance: Roles of Slit-Robo Signaling in Neocortical Formation. Front. Cell Dev. Biol. 8.

Gouwens, N.W., Sorensen, S.A., Baftizadeh, F., Budzillo, A., Lee, B.R., Jarsky, T., Alfiler, L., Baker, K., Barkan, E., Berry, K., Bertagnolli, D., Bickley, K., Bomben, J., Braun, T., Brouner, K., Casper, T., Crichton, K., Daigle, T.L., Dalley, R., de Frates, R.A., Dee, N., Desta, T., Lee, S.D., Dotson, N., Egdorf, T., Ellingwood, L., Enstrom, R., Esposito, L., Farrell, C., Feng, D., Fong, O., Gala, R., Gamlin, C., Gary, A., Glandon, A., Goldy, J., Gorham, M., Graybuck, L., Gu, H., Hadley, K., Hawrylycz, M.J., Henry, A.M., Hill, D., Hupp, M., Kebede, S., Kim, T.K., Kim, L., Kroll, M., Lee, C., Link, K.E., Mallory, M., Mann, R., Maxwell, M., McGraw, M., McMillen, D., Mukora, A., Ng, Lindsay, Ng, Lydia, Ngo, K., Nicovich, P.R., Oldre, A., Park, D., Peng, H., Penn, O., Pham, T., Pom, A., Popović, Z., Potekhina, L., Rajanbabu, R., Ransford, S., Reid, D., Rimorin, C., Robertson, M., Ronellenfitch, K., Ruiz, A., Sandman, D., Smith, K., Sulc, J., Sunkin, S.M., Szafer, A., Tieu, M., Torkelson, A., Trinh, J., Tung, H., Wakeman, W., Ward, K., Williams, G., Zhou, Z., Ting, J.T., Arkhipov, A., Sümbül, U., Lein, E.S., Koch, C., Yao, Z., Tasic, B., Berg, J., Murphy, G.J., Zeng, H., 2020. Integrated Morphoelectric and Transcriptomic Classification of Cortical GABAergic Cells. Cell 183, 935-953.e19. https://doi.org/10.1016/j.cell.2020.09.057

Harwell, C.C., Fuentealba, L.C., Gonzalez-Cerrillo, A., Parker, P.R.L., Gertz, C.C., Mazzola, E., Garcia, M.T., Alvarez-Buylla, A., Cepko, C.L., Kriegstein, A.R., 2015. Wide Dispersion and Diversity of Clonally

Related Inhibitory Interneurons. Neuron 87, 999–1007. https://doi.org/10.1016/j.neuron.2015.07.030

Hashimoto, M., Brito, S.I., Venner, A., Pasqualini, A.L., Yang, T.L., Allen, D., Stankowicz, S.J., Fuller, P.M., Anthony, T.E., 2022. Lateral septum modulates cortical state to tune responsivity to threat stimuli. Cell Rep. 41, 111521. https://doi.org/10.1016/j.celrep.2022.111521

Hayashi, Y., Majewska, A.K., 2005. Dendritic Spine Geometry: Functional Implication and Regulation. Neuron 46, 529–532. https://doi.org/10.1016/j.neuron.2005.05.006

Herriges, M.J., Swarr, D.T., Morley, M.P., Rathi, K.S., Peng, T., Stewart, K.M., Morrisey, E.E., 2014. Long noncoding RNAs are spatially correlated with transcription factors and regulate lung development. Genes Dev. 28, 1363–1379. https://doi.org/10.1101/gad.238782.114

Herriges, M.J., Tischfield, D.J., Cui, Z., Morley, M.P., Han, Y., Babu, A., Li, S., Lu, M., Cendan, I., Garcia, B.A., Anderson, S.A., Morrisey, E.E., 2017. The NANCI–Nkx2.1 gene duplex buffers Nkx2.1 expression to maintain lung development and homeostasis. Genes Dev. 31, 889–903. https://doi.org/10.1101/gad.298018.117

Hibino, H., Inanobe, A., Furutani, K., Murakami, S., Findlay, I., Kurachi, Y., 2010. Inwardly Rectifying Potassium Channels: Their Structure, Function, and Physiological Roles. Physiol. Rev. 90, 291–366. https://doi.org/10.1152/physrev.00021.2009

Hu, H., 1999. Chemorepulsion of Neuronal Migration by Slit2 in the Developing Mammalian Forebrain. Neuron 23, 703–711. https://doi.org/10.1016/S0896-6273(01)80029-5

Inoue, T., Ota, M., Ogawa, M., Mikoshiba, K., Aruga, J., 2007. Zic1 and Zic3 Regulate Medial Forebrain Development through Expansion of Neuronal Progenitors. J. Neurosci. 27, 5461–5473. https://doi.org/10.1523/JNEUROSCI.4046-06.2007

Jin, S., Guerrero-Juarez, C.F., Zhang, L., Chang, I., Ramos, R., Kuan, C.-H., Myung, P., Plikus, M.V., Nie, Q., 2021. Inference and analysis of cell-cell communication using CellChat. Nat. Commun. 12, 1088. https://doi.org/10.1038/s41467-021-21246-9

Katayama, S., Tomaru, Y., Kasukawa, T., Waki, K., Nakanishi, M., Nakamura, M., Nishida, H., Yap, C.C., Suzuki, M., Kawai, J., Suzuki, H., Carninci, P., Hayashizaki, Y., Wells, C., Frith, M., Ravasi, T., Pang, K.C., Hallinan, J., Mattick, J., Hume, D.A., Lipovich, L., Batalov, S., Engström, P.G., Mizuno, Y., Faghihi, M.A., Sandelin, A., Chalk, A.M., Mottagui-Tabar, S., Liang, Z., Lenhard, B., Wahlestedt, C., 2005. Antisense Transcription in the Mammalian Transcriptome. Science 309, 1564–1566. https://doi.org/10.1126/science.1112009

Kehoe, L.A., Bellone, C., Roo, M.D., Zandueta, A., Dey, P.N., Pérez-Otaño, I., Muller, D., 2014. GluN3A Promotes Dendritic Spine Pruning and Destabilization during Postnatal Development. J. Neurosci. 34, 9213–9221. https://doi.org/10.1523/JNEUROSCI.5183-13.2014

Kim, D.W., Washington, P.W., Wang, Z.Q., Lin, S.H., Sun, C., Ismail, B.T., Wang, H., Jiang, L., Blackshaw, S., 2020. The cellular and molecular landscape of hypothalamic patterning and differentiation from embryonic to late postnatal development. Nat. Commun. 11, 4360. https://doi.org/10.1038/s41467-020-18231-z

Lein, E.S., Hawrylycz, M.J., Ao, N., Ayres, M., Bensinger, A., Bernard, A., Boe, A.F., Boguski, M.S., Brockway, K.S., Byrnes, E.J., Chen, Lin, Chen, Li, Chen, T.-M., Chi Chin, M., Chong, J., Crook, B.E., Czaplinska, A., Dang, C.N., Datta, S., Dee, N.R., Desaki, A.L., Desta, T., Diep, E., Dolbeare, T.A., Donelan, M.J., Dong, H.-W., Dougherty, J.G., Duncan, B.J., Ebbert, A.J., Eichele, G., Estin, L.K., Faber, C., Facer, B.A., Fields, R., Fischer, S.R., Fliss, T.P., Frensley, C., Gates, S.N., Glattfelder, K.J., Halverson, K.R., Hart, M.R., Hohmann, J.G., Howell, M.P., Jeung, D.P., Johnson, R.A., Karr, P.T., Kawal, R., Kidney, J.M., Knapik, R.H., Kuan, C.L., Lake, J.H., Laramee, A.R., Larsen, K.D., Lau, C., Lemon, T.A., Liang, A.J., Liu, Y., Luong, L.T., Michaels, J., Morgan, J.J., Morgan, R.J., Mortrud, M.T., Mosqueda, N.F., Ng, L.L., Ng, R., Orta, G.J., Overly, C.C., Pak, T.H., Parry, S.E., Pathak, S.D., Pearson, O.C., Puchalski, R.B., Riley, Z.L., Rockett, H.R., Rowland, S.A., Royall, J.J., Ruiz, M.J.,

Sarno, N.R., Schaffnit, K., Shapovalova, N.V., Sivisay, T., Slaughterbeck, C.R., Smith, S.C., Smith, K.A., Smith, B.I., Sodt, A.J., Stewart, N.N., Stumpf, K.-R., Sunkin, S.M., Sutram, M., Tam, A., Teemer, C.D., Thaller, C., Thompson, C.L., Varnam, L.R., Visel, A., Whitlock, R.M., Wohnoutka, P.E., Wolkey, C.K., Wong, V.Y., Wood, M., Yaylaoglu, M.B., Young, R.C., Youngstrom, B.L., Feng Yuan, X., Zhang, B., Zwingman, T.A., Jones, A.R., 2007. Genome-wide atlas of gene expression in the adult mouse brain. Nature 445, 168–176. https://doi.org/10.1038/nature05453

Leranth, C., Frotscher, M., 1989. Organization of the septal region in the rat brain: Cholinergic-GABAergic interconnections and the termination of hippocampo-septal fibers. J. Comp. Neurol. 289, 304–314. https://doi.org/10.1002/cne.902890210

Li, H., Sung, H.H., Lau, C.G., 2022. Activation of Somatostatin-Expressing Neurons in the Lateral Septum Improves Stress-Induced Depressive-like Behaviors in Mice. Pharmaceutics 14, 2253. https://doi.org/10.3390/pharmaceutics14102253

Li, L., Durand-de Cuttoli, R., Aubry, A.V., Burnett, C.J., Cathomas, F., Parise, L.F., Chan, K.L., Morel, C., Yuan, C., Shimo, Y., Lin, H., Wang, J., Russo, S.J., 2023. Social trauma engages lateral septum circuitry to occlude social reward. Nature 613, 696–703. https://doi.org/10.1038/s41586-022-05484-5

Magno, L., Barry, C., Schmidt-Hieber, C., Theodotou, P., Häusser, M., Kessaris, N., 2017. NKX2-1 Is Required in the Embryonic Septum for Cholinergic System Development, Learning, and Memory. Cell Rep. 20, 1572–1584. https://doi.org/10.1016/j.celrep.2017.07.053

Mao, B.-Q., MacLeish, P.R., Victor, J.D., 2003. Role of Hyperpolarization-Activated Currents for the Intrinsic Dynamics of Isolated Retinal Neurons. Biophys. J. 84, 2756–2767. https://doi.org/10.1016/S0006-3495(03)75080-2

Mayer, C., Hafemeister, C., Bandler, R.C., Machold, R., Batista Brito, R., Jaglin, X., Allaway, K., Butler, A., Fishell, G., Satija, R., 2018. Developmental diversification of cortical inhibitory interneurons. Nature 555, 457–462. https://doi.org/10.1038/nature25999

Mayer, C., Jaglin, X.H., Cobbs, L.V., Bandler, R.C., Streicher, C., Cepko, C.L., Hippenmeyer, S., Fishell, G., 2015. Clonally Related Forebrain Interneurons Disperse Broadly across Both Functional Areas and Structural Boundaries. Neuron 87, 989–998. https://doi.org/10.1016/j.neuron.2015.07.011

Menon, R., Süß, T., Oliveira, V.E. de M., Neumann, I.D., Bludau, A., 2022. Neurobiology of the lateral septum: regulation of social behavior. Trends Neurosci. 45, 27–40. https://doi.org/10.1016/j.tins.2021.10.010

Minocha, S., Valloton, D., Ypsilanti, A.R., Fiumelli, H., Allen, E.A., Yanagawa, Y., Marin, O., Chédotal, A., Hornung, J.-P., Lebrand, C., 2015. Nkx2.1-derived astrocytes and neurons together with Slit2 are indispensable for anterior commissure formation. Nat. Commun. 6, 6887. https://doi.org/10.1038/ncomms7887

Mo, A., Mukamel, E.A., Davis, F.P., Luo, C., Henry, G.L., Picard, S., Urich, M.A., Nery, J.R., Sejnowski, T.J., Lister, R., Eddy, S.R., Ecker, J.R., Nathans, J., 2015. Epigenomic Signatures of Neuronal Diversity in the Mammalian Brain. Neuron 86, 1369–1384. https://doi.org/10.1016/j.neuron.2015.05.018

Moens, C.B., Selleri, L., 2006. Hox cofactors in vertebrate development. Dev. Biol. 291, 193–206. https://doi.org/10.1016/j.ydbio.2005.10.032

Moerman, T., Aibar Santos, S., Bravo González-Blas, C., Simm, J., Moreau, Y., Aerts, J., Aerts, S., 2019. GRNBoost2 and Arboreto: efficient and scalable inference of gene regulatory networks. Bioinformatics 35, 2159–2161. https://doi.org/10.1093/bioinformatics/bty916

Moffitt, J.R., Bambah-Mukku, D., Eichhorn, S.W., Vaughn, E., Shekhar, K., Perez, J.D., Rubinstein, N.D., Hao, J., Regev, A., Dulac, C., Zhuang, X., 2018. Molecular, spatial, and functional single-cell profiling of the hypothalamic preoptic region. Science 362, eaau5324. https://doi.org/10.1126/science.aau5324

Nishimura-Akiyoshi, S., Niimi, K., Nakashiba, T., Itohara, S., 2007. Axonal netrin-Gs transneuronally determine lamina-specific subdendritic segments. Proc. Natl. Acad. Sci. 104, 14801–14806. https://doi.org/10.1073/pnas.0706919104

Nóbrega-Pereira, S., Kessaris, N., Du, T., Kimura, S., Anderson, S.A., Marín, O., 2008. Postmitotic Nkx2-1 Controls the Migration of Telencephalic Interneurons by Direct Repression of Guidance Receptors. Neuron 59, 733–745. https://doi.org/10.1016/j.neuron.2008.07.024

Pachitariu, M., Stringer, C., 2022. Cellpose 2.0: how to train your own model. Nat. Methods 19, 1634–1641. https://doi.org/10.1038/s41592-022-01663-4

Park, M., Vorperian, S., Wang, S., Pisco, A.O., 2020. Single-cell identity definition using random forests and recursive feature elimination. https://doi.org/10.1101/2020.08.03.233650

Pchitskaya, E., Bezprozvanny, I., 2020. Dendritic Spines Shape Analysis—Classification or Clusterization? Perspective. Front. Synaptic Neurosci. 12.

Peng, H., Xie, P., Liu, L., Kuang, X., Wang, Yimin, Qu, L., Gong, H., Jiang, S., Li, A., Ruan, Z., Ding, L., Yao, Z., Chen, C., Chen, M., Daigle, T.L., Dalley, R., Ding, Z., Duan, Y., Feiner, A., He, P., Hill, C., Hirokawa, K.E., Hong, G., Huang, L., Kebede, S., Kuo, H.-C., Larsen, R., Lesnar, P., Li, L., Li, Q., Li, X., Li, Yaoyao, Li, Yuanyuan, Liu, A., Lu, D., Mok, S., Ng, L., Nguyen, T.N., Ouyang, Q., Pan, J., Shen, E., Song, Y., Sunkin, S.M., Tasic, B., Veldman, M.B., Wakeman, W., Wan, W., Wang, P., Wang, Q., Wang, T., Wang, Yaping, Xiong, F., Xiong, W., Xu, W., Ye, M., Yin, L., Yu, Y., Yuan, Jia, Yuan, Jing, Yun, Z., Zeng, S., Zhang, S., Zhao, S., Zhao, Z., Zhou, Z., Huang, Z.J., Esposito, L., Hawrylycz, M.J., Sorensen, S.A., Yang, X.W., Zheng, Y., Gu, Z., Xie, W., Koch, C., Luo, Q., Harris, J.A., Wang, Yun, Zeng, H., 2021. Morphological diversity of single neurons in molecularly defined cell types. Nature 598, 174–181. https://doi.org/10.1038/s41586-021-03941-1

Polański, K., Young, M.D., Miao, Z., Meyer, K.B., Teichmann, S.A., Park, J.-E., 2020. BBKNN: fast batch alignment of single cell transcriptomes. Bioinformatics 36, 964–965. https://doi.org/10.1093/bioinformatics/btz625

Raisman, G., 1969. Neuronal plasticity in the septal nuclei of the adult rat. Brain Res. 14, 25–48. https://doi.org/10.1016/0006-8993(69)90029-8

Raisman, G., 1966. THE CONNEXIONS OF THE SEPTUM. Brain 89, 317–348. https://doi.org/10.1093/brain/89.2.317

Rajmohan, V., Mohandas, E., 2007. The limbic system. Indian J. Psychiatry 49, 132. https://doi.org/10.4103/0019-5545.33264

Risold, P.Y., Swanson, L.W., 1997. Connections of the rat lateral septal complex1Published on the World Wide Web on 2 June 1997.1. Brain Res. Rev. 24, 115–195. https://doi.org/10.1016/S0165-0173(97)00009-X

Rizzi-Wise, C.A., Wang, D.V., 2021. Putting Together Pieces of the Lateral Septum: Multifaceted Functions and Its Neural Pathways. eNeuro 8. https://doi.org/10.1523/ENEURO.0315-21.2021

Sandberg, M., Flandin, P., Silberberg, S., Su-Feher, L., Price, J.D., Hu, J.S., Kim, C., Visel, A., Nord, A.S., Rubenstein, J.L.R., 2016. Transcriptional Networks Controlled by NKX2-1 in the Development of Forebrain GABAergic Neurons. Neuron 91, 1260–1275. https://doi.org/10.1016/j.neuron.2016.08.020

Seal, R.L., Braschi, B., Gray, K., Jones, T.E.M., Tweedie, S., Haim-Vilmovsky, L., Bruford, E.A., 2023. Genenames.org: the HGNC resources in 2023. Nucleic Acids Res. 51, D1003–D1009. https://doi.org/10.1093/nar/gkac888

Sheehan, T.P., Chambers, R.A., Russell, D.S., 2004. Regulation of affect by the lateral septum: implications for neuropsychiatry. Brain Res. Rev. 46, 71–117. https://doi.org/10.1016/j.brainresrev.2004.04.009

Shin, S., Pribiag, H., Lilascharoen, V., Knowland, D., Wang, X.-Y., Lim, B.K., 2018. Drd3 Signaling in the Lateral Septum Mediates Early Life Stress-Induced Social Dysfunction. Neuron 97, 195-208.e6. https://doi.org/10.1016/j.neuron.2017.11.040

Short, A.K., Thai, C.W., Chen, Y., Kamei, N., Pham, A.L., Birnie, M.T., Bolton, J.L., Mortazavi, A., Baram, T.Z., 2023. Single-Cell Transcriptional Changes in Hypothalamic Corticotropin-Releasing Factor–Expressing Neurons After Early-Life Adversity Inform Enduring Alterations in Vulnerabilities to Stress. Biol. Psychiatry Glob. Open Sci. 3, 99–109. https://doi.org/10.1016/j.bpsgos.2021.12.006

Simon, R.C., Fleming, W.T., Senthilkumar, P., Briones, B.A., Ishii, K.K., Hjort, M.M., Martin, M.M., Hashikawa, K., Sanders, A.D., Golden, S.A., Stuber, G.D., 2024. Opioid-driven disruption of the septal complex reveals a role for neurotensin-expressing neurons in withdrawal. https://doi.org/10.1101/2024.01.15.575766

Sivaramakrishnan, S., Oliver, D.L., 2001. Distinct K Currents Result in Physiologically Distinct Cell Types in the Inferior Colliculus of the Rat. J. Neurosci. 21, 2861–2877. https://doi.org/10.1523/JNEUROSCI.21-08-02861.2001

Sokolowski, K., Corbin, J., 2012. Wired for behaviors: from development to function of innate limbic system circuitry. Front. Mol. Neurosci. 5.

Sonoda, T., Mochizuki, C., Yamashita, T., Watanabe-Kaneko, K., Miyagi, Y., Shigeri, Y., Yazama, F., Okuda, K., Kawamoto, S., 2006. Binding of glutamate receptor δ2 to its scaffold protein, Delphilin, is regulated by PKA. Biochem. Biophys. Res. Commun. 350, 748–752. https://doi.org/10.1016/j.bbrc.2006.09.109

Su, Z., Wang, Z., Lindtner, S., Yang, L., Shang, Z., Tian, Y., Guo, R., You, Y., Zhou, W., Rubenstein, J.L., Yang, Z., Zhang, Z., 2022. Dlx1/2-dependent expression of Meis2 promotes neuronal fate determination in the mammalian striatum. Development 149, dev200035. https://doi.org/10.1242/dev.200035

Svensson, V., Teichmann, S.A., Stegle, O., 2018. SpatialDE: identification of spatially variable genes. Nat. Methods 15, 343–346. https://doi.org/10.1038/nmeth.4636

Swanson, L.W., Cowan, W.M., 1979. The connections of the septal region in the rat. J. Comp. Neurol. 186, 621–655. https://doi.org/10.1002/cne.901860408

Tasic, B., Menon, V., Nguyen, T.N., Kim, T.K., Jarsky, T., Yao, Z., Levi, B., Gray, L.T., Sorensen, S.A., Dolbeare, T., Bertagnolli, D., Goldy, J., Shapovalova, N., Parry, S., Lee, C., Smith, K., Bernard, A., Madisen, L., Sunkin, S.M., Hawrylycz, M., Koch, C., Zeng, H., 2016. Adult mouse cortical cell taxonomy revealed by single cell transcriptomics. Nat. Neurosci. 19, 335–346. https://doi.org/10.1038/nn.4216

Tian, J., Thakur, D.P., Lu, Y., Zhu, Y., Freichel, M., Flockerzi, V., Zhu, M.X., 2014. Dual depolarization responses generated within the same lateral septal neurons by TRPC4-containing channels. Pflüg. Arch. - Eur. J. Physiol. 466, 1301–1316. https://doi.org/10.1007/s00424-013-1362-5

Turrero García, M., Harwell, C.C., 2017. Radial glia in the ventral telencephalon. FEBS Lett. 591, 3942–3959. https://doi.org/10.1002/1873-3468.12829

Turrero García, M., Stegmann, S.K., Lacey, T.E., Reid, C.M., Hrvatin, S., Weinreb, C., Adam, M.A., Nagy, M.A., Harwell, C.C., 2021. Transcriptional profiling of sequentially generated septal neuron fates. eLife 10, e71545. https://doi.org/10.7554/eLife.71545

Turrero García, M., Tran, D.N., Peterson, R.E., Stegmann, S.K., Hanson, S.M., Reid, C.M., Xie, Y., Vu, S., Harwell, C.C., 2023. A developmentally defined population of neurons in the lateral septum controls responses to aversive stimuli. https://doi.org/10.1101/2023.09.24.559205

Wang, Y., Krabbe, S., Eddison, M., Henry, F.E., Fleishman, G., Lemire, A.L., Wang, L., Korff, W., Tillberg, P.W., Lüthi, A., Sternson, S.M., 2023. Multimodal mapping of cell types and projections in the central nucleus of the amygdala. eLife 12, e84262. https://doi.org/10.7554/eLife.84262

Wei, B., Huang, Z., He, S., Sun, C., You, Y., Liu, F., Yang, Z., 2012. The onion skin-like organization of the septum arises from multiple embryonic origins to form multiple adult neuronal fates. Neuroscience 222, 110–123. https://doi.org/10.1016/j.neuroscience.2012.07.016

Wirtshafter, H.S., Wilson, M.A., 2021. Lateral septum as a nexus for mood, motivation, and movement. Neurosci. Biobehav. Rev. 126, 544–559. https://doi.org/10.1016/j.neubiorev.2021.03.029

Wirtshafter, H.S., Wilson, M.A., 2020. Differences in reward biased spatial representations in the lateral septum and hippocampus. eLife 9, e55252. https://doi.org/10.7554/eLife.55252

Wolf, F.A., Angerer, P., Theis, F.J., 2018. SCANPY: large-scale single-cell gene expression data analysis. Genome Biol. 19, 15. https://doi.org/10.1186/s13059-017-1382-0

Wu, T., Hu, E., Xu, S., Chen, M., Guo, P., Dai, Z., Feng, T., Zhou, L., Tang, W., Zhan, L., Fu, X., Liu, S., Bo, X., Yu, G., 2021. clusterProfiler 4.0: A universal enrichment tool for interpreting omics data. The Innovation 2, 100141. https://doi.org/10.1016/j.xinn.2021.100141

Xie, Y., Reid, C.M., Granados, A.A., Garcia, M.T., Dale-Huang, F., Hanson, S.M., Mancia, W., Liu, J., Adam, M., Mosto, O., Pisco, A.O., Alvarez-Buylla, A., Harwell, C.C., 2023. Developmental origin and local signals cooperate to determine septal astrocyte identity. https://doi.org/10.1101/2023.10.08.561428

Yao, Z., van Velthoven, C.T.J., Kunst, M., Zhang, M., McMillen, D., Lee, C., Jung, W., Goldy, J., Abdelhak, A., Aitken, M., Baker, K., Baker, P., Barkan, E., Bertagnolli, D., Bhandiwad, A., Bielstein, C., Bishwakarma, P., Campos, J., Carey, D., Casper, T., Chakka, A.B., Chakrabarty, R., Chavan, S., Chen, M., Clark, M., Close, J., Crichton, K., Daniel, S., DiValentin, P., Dolbeare, T., Ellingwood, L., Fiabane, E., Fliss, T., Gee, J., Gerstenberger, J., Glandon, A., Gloe, J., Gould, J., Gray, J., Guilford, N., Guzman, J., Hirschstein, D., Ho, W., Hooper, M., Huang, M., Hupp, M., Jin, K., Kroll, M., Lathia, K., Leon, A., Li, S., Long, B., Madigan, Z., Malloy, J., Malone, J., Maltzer, Z., Martin, N., McCue, R., McGinty, R., Mei, N., Melchor, J., Meyerdierks, E., Mollenkopf, T., Moonsman, S., Nguyen, T.N., Otto, S., Pham, T., Rimorin, C., Ruiz, A., Sanchez, R., Sawyer, L., Shapovalova, N., Shepard, N., Slaughterbeck, C., Sulc, J., Tieu, M., Torkelson, A., Tung, H., Valera Cuevas, N., Vance, S., Wadhwani, K., Ward, K., Levi, B., Farrell, C., Young, R., Staats, B., Wang, M.-Q.M., Thompson, C.L., Mufti, S., Pagan, C.M., Kruse, L., Dee, N., Sunkin, S.M., Esposito, L., Hawrylycz, M.J., Waters, J., Ng, L., Smith, K., Tasic, B., Zhuang, X., Zeng, H., 2023. A high-resolution transcriptomic and spatial atlas of cell types in the whole mouse brain. Nature 624, 317–332. https://doi.org/10.1038/s41586-023-06812-z

Yao, Z., van Velthoven, C.T.J., Nguyen, T.N., Goldy, J., Sedeno-Cortes, A.E., Baftizadeh, F., Bertagnolli, D., Casper, T., Chiang, M., Crichton, K., Ding, S.-L., Fong, O., Garren, E., Glandon, A., Gouwens, N.W., Gray, J., Graybuck, L.T., Hawrylycz, M.J., Hirschstein, D., Kroll, M., Lathia, K., Lee, C., Levi, B., McMillen, D., Mok, S., Pham, T., Ren, Q., Rimorin, C., Shapovalova, N., Sulc, J., Sunkin, S.M., Tieu, M., Torkelson, A., Tung, H., Ward, K., Dee, N., Smith, K.A., Tasic, B., Zeng, H., 2021. A taxonomy of transcriptomic cell types across the isocortex and hippocampal formation. Cell 184, 3222-3241.e26. https://doi.org/10.1016/j.cell.2021.04.021

Yu, G., 2020. Gene Ontology Semantic Similarity Analysis Using GOSemSim, in: Kidder, B.L. (Ed.), Stem Cell Transcriptional Networks: Methods and Protocols, Methods in Molecular Biology. Springer US, New York, NY, pp. 207–215. https://doi.org/10.1007/978-1-0716-0301-7_11

Zeisel, A., Muñoz-Manchado, A.B., Codeluppi, S., Lönnerberg, P., La Manno, G., Juréus, A., Marques, S., Munguba, H., He, L., Betsholtz, C., Rolny, C., Castelo-Branco, G., Hjerling-Leffler, J., Linnarsson, S., 2015. Cell types in the mouse cortex and hippocampus revealed by single-cell RNA-seq. Science 347, 1138–1142. https://doi.org/10.1126/science.aaa1934

Zeng, H., 2022. What is a cell type and how to define it? Cell 185, 2739–2755. https://doi.org/10.1016/j.cell.2022.06.031

Zhang, M., Pan, X., Jung, W., Halpern, A.R., Eichhorn, S.W., Lei, Z., Cohen, L., Smith, K.A., Tasic, B., Yao, Z., Zeng, H., Zhuang, X., 2023. Molecularly defined and spatially resolved cell atlas of the whole mouse brain. Nature 624, 343–354. https://doi.org/10.1038/s41586-023-06808-9

Zhang, Q., Sano, C., Masuda, A., Ando, R., Tanaka, M., Itohara, S., 2016. Netrin-G1 regulates fear-like and anxiety-like behaviors in dissociable neural circuits. Sci. Rep. 6, 28750. https://doi.org/10.1038/srep28750

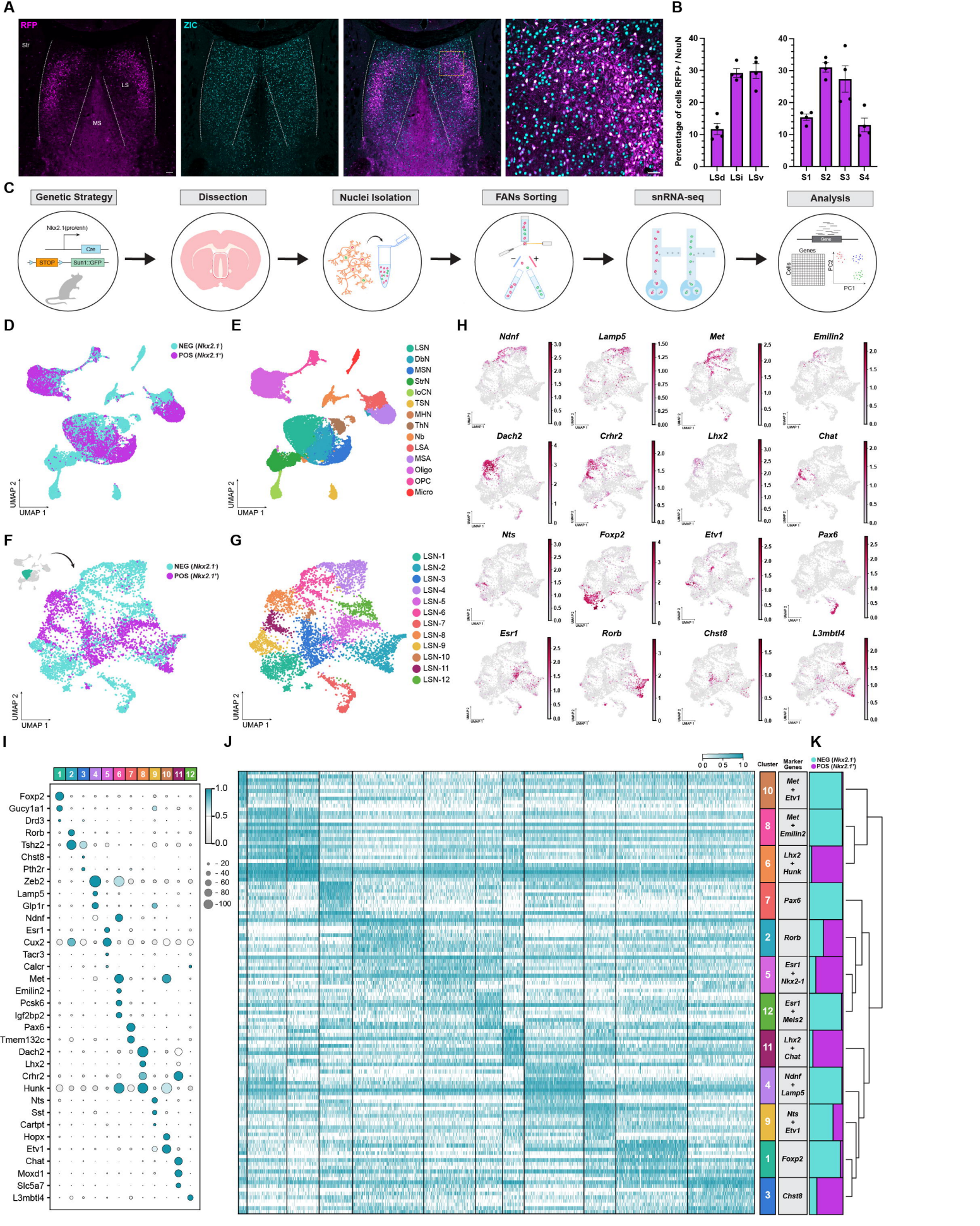
A
RFP
Str
LS
MS
ZIC
B
Percentage of cells RFP+ / NeuN
LSd
LSi
LSv
S1
S2
S3
S4
C
Genetic Strategy
Dissection
Nuclei Isolation
FANs Sorting
snRNA-seq
Analysis
Nkx2.1(pro/enh)
Cre
STOP
Sun1::GFP
Gene
Genes
Cells
PC2
PC1
D
NEG (Nkx2.1-)
POS (Nkx2.1+)
UMAP 2
UMAP 1
E
LSN
DbN
MSN
StrN
IoCN
TSN
MHN
ThN
Nb
LSA
MSA
Oligo
OPC
Micro
F
G
LSN-1
LSN-2
LSN-3
LSN-4
LSN-5
LSN-6
LSN-7
LSN-8
LSN-9
LSN-10
LSN-11
LSN-12
H
Ndnf
Lamp5
Met
Emilin2
Dach2
Crhr2
Lhx2
Chat
Nts
Foxp2
Etv1
Pax6
Esr1
Rorb
Chst8
L3mbtl4
I
Foxp2
Gucy1a1
Drd3
Rorb
Tshz2
Chst8
Pth2r
Zeb2
Lamp5
Glp1r
Ndnf
Esr1
Cux2
Tacr3
Calcr
Met
Emilin2
Pcsk6
Igf2bp2
Pax6
Tmem132c
Dach2
Lhx2
Crhr2
Hunk
Nts
Sst
Cartpt
Hopx
Etv1
Chat
Moxd1
Slc5a7
L3mbtl4
J
Cluster
Marker Genes
K
NEG (Nkx2.1-)
POS (Nkx2.1+)
Met + Etv1
Met + Emilin2
Lhx2 + Hunk
Pax6
Rorb
Esr1 + Nkx2-1
Esr1 + Meis2
Lhx2 + Chat
Ndnf + Lamp5
Nts + Etv1
Foxp2
Chst8

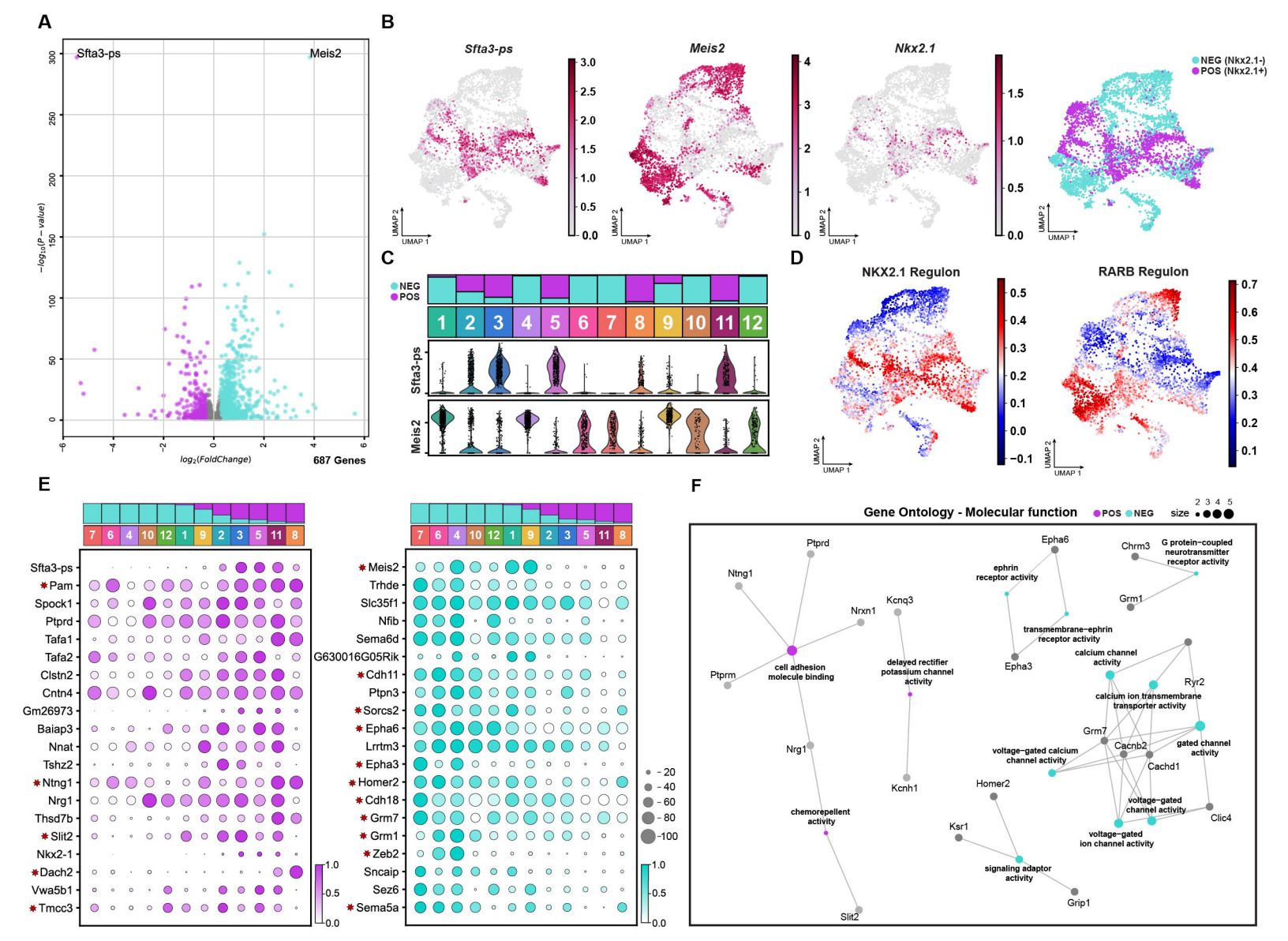
A
Sfta3-ps
Meis2
687 Genes
B
Sfta3-ps
Meis2
Nkx2.1
NEG (Nkx2.1-)
POS (Nkx2.1+)
C
NEG
POS
Sfta3-ps
Meis2
D
NKX2.1 Regulon
RARB Regulon
E
Sfta3-ps
Pam
Spock1
Ptprd
Tafa1
Tafa2
Clstn2
Cntn4
Gm26973
Baiap3
Nnat
Tshz2
Ntng1
Nrg1
Thsd7b
Slit2
Nkx2-1
Dach2
Vwa5b1
Tmcc3
Meis2
Trhde
Slc35f1
Nfib
Sema6d
G630016G05Rik
Cdh11
Ptpn3
Sorcs2
Epha6
Lrrtm3
Epha3
Homer2
Cdh18
Grm7
Grm1
Zeb2
Sncaip
Sez6
Sema5a
F
Gene Ontology - Molecular function
POS
NEG
size
Ptprd
Ntng1
Nrxn1
Kcnq3
Ptprm
cell adhesion molecule binding
delayed rectifier potassium channel activity
Nrg1
Kcnh1
chemorepellent activity
Slit2
Epha6
ephrin receptor activity
Chrm3
G protein−coupled neurotransmitter receptor activity
Grm1
transmembrane−ephrin receptor activity
Epha3
calcium channel activity
Ryr2
calcium ion transmembrane transporter activity
Grm7
Cacnb2
gated channel activity
voltage−gated calcium channel activity
Cachd1
Homer2
voltage−gated channel activity
Clic4
Ksr1
voltage−gated ion channel activity
signaling adaptor activity
Grip1

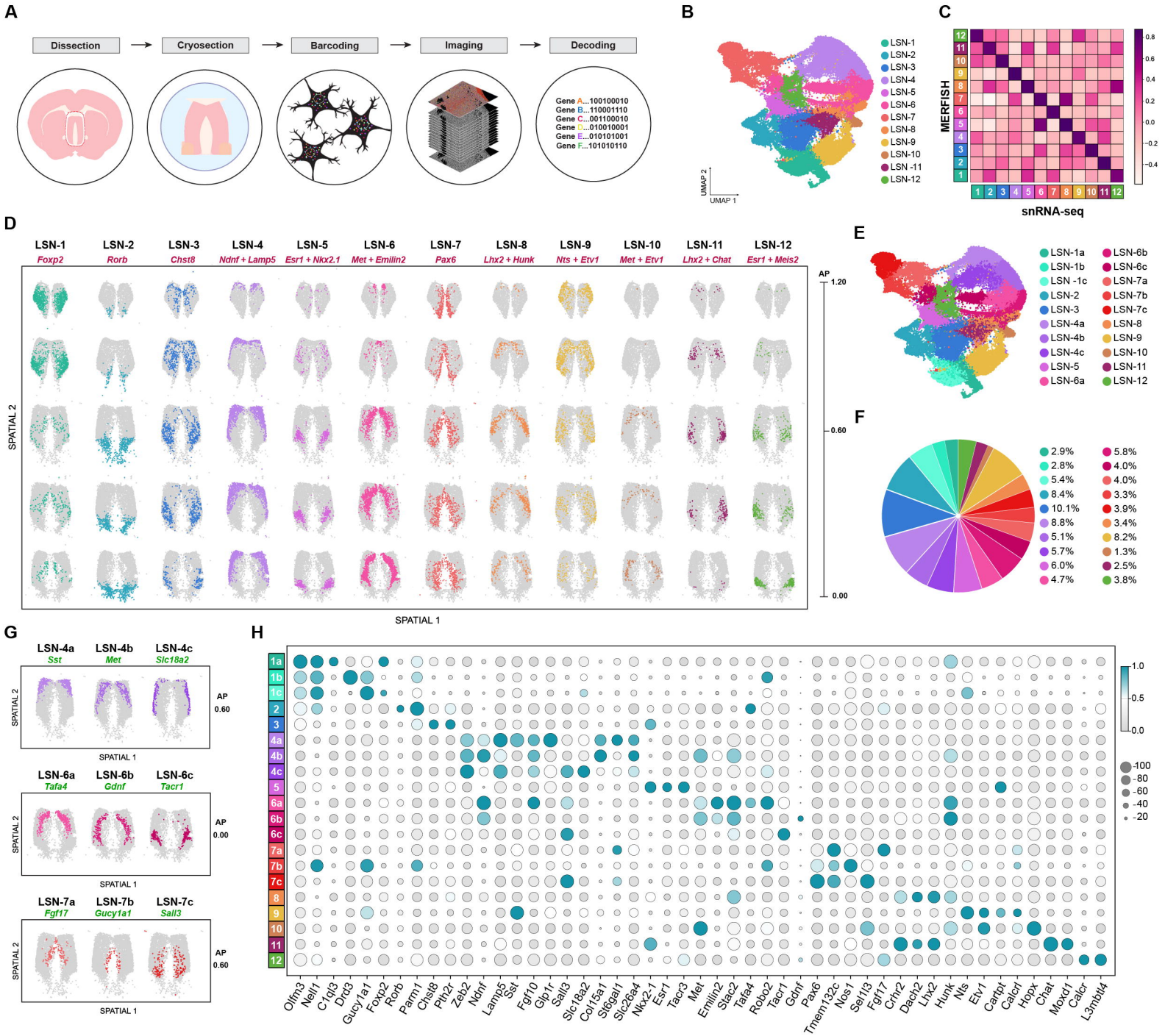
A
Dissection
Cryosection
Barcoding
Imaging
Decoding
Gene A...100100010
Gene B...110001110
Gene C...001100010
Gene D...010010001
Gene E...010101001
Gene F...101010110
B
LSN-1
LSN-2
LSN-3
LSN-4
LSN-5
LSN-6
LSN-7
LSN-8
LSN-9
LSN-10
LSN -11
LSN-12
UMAP 2
UMAP 1
C
MERFISH
snRNA-seq
D
LSN-1 Foxp2
LSN-2 Rorb
LSN-3 Chst8
LSN-4 Ndnf + Lamp5
LSN-5 Esr1 + Nkx2.1
LSN-6 Met + Emilin2
LSN-7 Pax6
LSN-8 Lhx2 + Hunk
LSN-9 Nts + Etv1
LSN-10 Met + Etv1
LSN-11 Lhx2 + Chat
LSN-12 Esr1 + Meis2
SPATIAL 2
SPATIAL 1
AP
1.20
0.60
0.00
E
LSN-1a
LSN-1b
LSN -1c
LSN-2
LSN-3
LSN-4a
LSN-4b
LSN-4c
LSN-5
LSN-6a
LSN-6b
LSN-6c
LSN-7a
LSN-7b
LSN-7c
LSN-8
LSN-9
LSN-10
LSN-11
LSN-12
F
2.9%
2.8%
5.4%
8.4%
10.1%
8.8%
5.1%
5.7%
6.0%
4.7%
5.8%
4.0%
4.0%
3.3%
3.9%
3.4%
8.2%
1.3%
2.5%
3.8%
G
LSN-4a Sst
LSN-4b Met
LSN-4c Slc18a2
LSN-6a Tafa4
LSN-6b Gdnf
LSN-6c Tacr1
LSN-7a Fgf17
LSN-7b Gucy1a1
LSN-7c Sall3
H
Olfm3
Nell1
C1ql3
Drd3
Gucy1a1
Foxp2
Rorb
Pamr1
Chst8
Pth2r
Zeb2
Ndnf
Lamp5
Sst
Fgf10
Glp1r
Sall3
Slc18a2
Col15a1
St6gal1
Slc26a4
Nkx2-1
Esr1
Tacr3
Met
Emilin2
Stac2
Tafa4
Robo2
Tacr1
Gdnf
Pax6
Tmem132c
Nos1
Sel1l3
Fgf17
Crhr2
Dach2
Lhx2
Hunk
Nts
Etv1
Cartpt
Calcrl
Hopx
Chat
Moxd1
Calcr
L3mbtl4

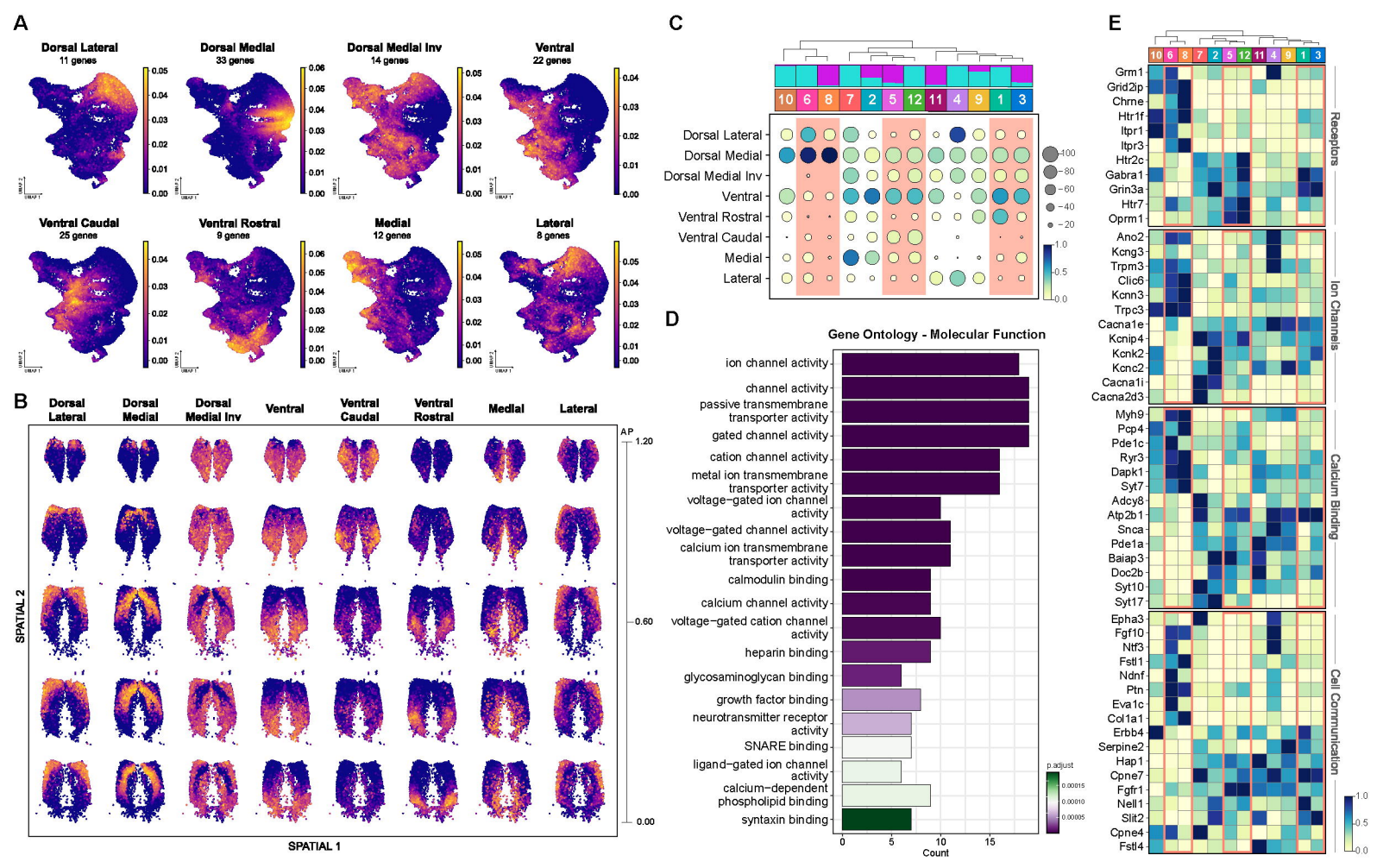
A
Dorsal Lateral
11 genes
Dorsal Medial
33 genes
Dorsal Medial Inv
14 genes
Ventral
22 genes
Ventral Caudal
25 genes
Ventral Rostral
9 genes
Medial
12 genes
Lateral
8 genes
B
Dorsal Lateral
Dorsal Medial
Dorsal Medial Inv
Ventral
Ventral Caudal
Ventral Rostral
Medial
Lateral
AP
1.20
0.60
0.00
SPATIAL 2
SPATIAL 1
C
10 6 8 7 2 5 12 11 4 9 1 3
Dorsal Lateral
Dorsal Medial
Dorsal Medial Inv
Ventral
Ventral Rostral
Ventral Caudal
Medial
Lateral
100
80
60
40
20
1.0
0.5
0.0
D
Gene Ontology - Molecular Function
ion channel activity
channel activity
passive transmembrane transporter activity
gated channel activity
cation channel activity
metal ion transmembrane transporter activity
voltage−gated ion channel activity
voltage−gated channel activity
calcium ion transmembrane transporter activity
calmodulin binding
calcium channel activity
voltage−gated cation channel activity
heparin binding
glycosaminoglycan binding
growth factor binding
neurotransmitter receptor activity
SNARE binding
ligand−gated ion channel activity
calcium−dependent phospholipid binding
syntaxin binding
0
5
10
15
Count
p.adjust
0.00015
0.00010
0.00005
E
10 6 8 7 2 5 12 11 4 9 1 3
Grm1
Grid2ip
Chrne
Htr1f
Itpr1
Itpr3
Htr2c
Gabra1
Grin3a
Htr7
Oprm1
Receptors
Ano2
Kcng3
Trpm3
Clic6
Kcnn3
Trpc3
Cacna1e
Kcnip4
Kcnk2
Kcnc2
Cacna1i
Cacna2d3
Ion Channels
Myh9
Pcp4
Pde1c
Ryr3
Dapk1
Syt7
Adcy8
Atp2b1
Snca
Pde1a
Baiap3
Doc2b
Syt10
Syt17
Calcium Binding
Epha3
Fgf10
Ntf3
Fstl1
Ndnf
Ptn
Eva1c
Col1a1
Erbb4
Serpine2
Hap1
Cpne7
Fgfr1
Nell1
Slit2
Cpne4
Fstl4
Cell Communication
1.0
0.5
0.0

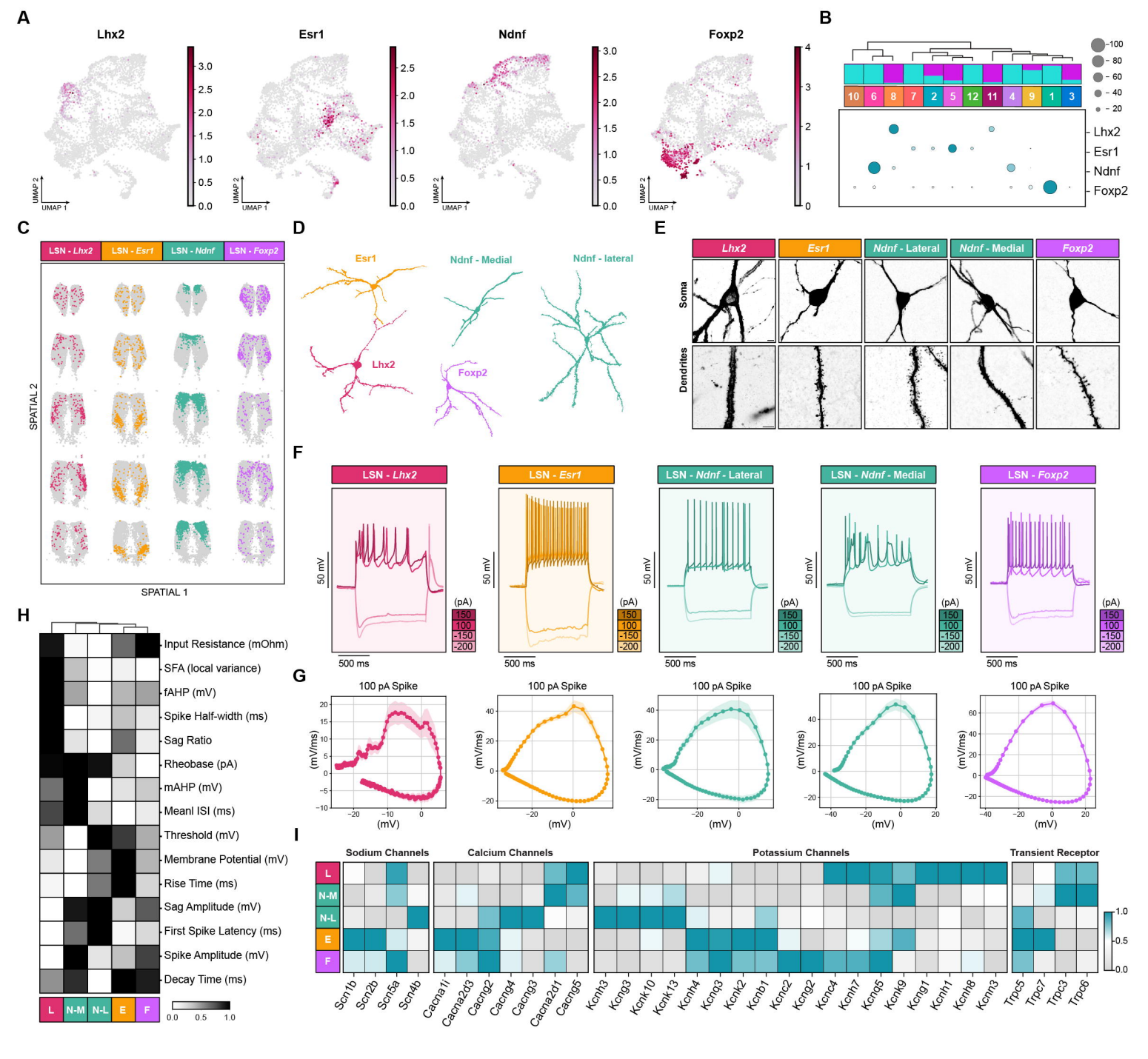
A
Lhx2
Esr1
Ndnf
Foxp2
UMAP 1
UMAP 2
B
10 6 8 7 2 5 12 11 4 9 1 3
Lhx2
Esr1
Ndnf
Foxp2
C
LSN - Lhx2
LSN - Esr1
LSN - Ndnf
LSN - Foxp2
SPATIAL 1
SPATIAL 2
D
Esr1
Ndnf - Medial
Ndnf - lateral
Lhx2
Foxp2
E
Lhx2
Esr1
Ndnf - Lateral
Ndnf - Medial
Foxp2
Soma
Dendrites
F
LSN - Lhx2
LSN - Esr1
LSN - Ndnf - Lateral
LSN - Ndnf - Medial
LSN - Foxp2
50 mV
500 ms
(pA)
150
100
-150
-200
G
100 pA Spike
(mV/ms)
(mV)
H
Input Resistance (mOhm)
SFA (local variance)
fAHP (mV)
Spike Half-width (ms)
Sag Ratio
Rheobase (pA)
mAHP (mV)
Meanl ISI (ms)
Threshold (mV)
Membrane Potential (mV)
Rise Time (ms)
Sag Amplitude (mV)
First Spike Latency (ms)
Spike Amplitude (mV)
Decay Time (ms)
L
N-M
N-L
E
F
I
Sodium Channels
Calcium Channels
Potassium Channels
Transient Receptor
Scn1b
Scn2b
Scn5a
Scn4b
Cacna1i
Cacna2d3
Cacng2
Cacng4
Cacng3
Cacna2d1
Cacng5
Kcnh3
Kcng3
Kcnk10
Kcnk13
Kcnh4
Kcnq3
Kcnk2
Kcnb1
Kcnc2
Kcng2
Kcnc4
Kcnh7
Kcnq5
Kcnk9
Kcng1
Kcnh1
Kcnh8
Kcnn3
Trpc5
Trpc7
Trpc3
Trpc6

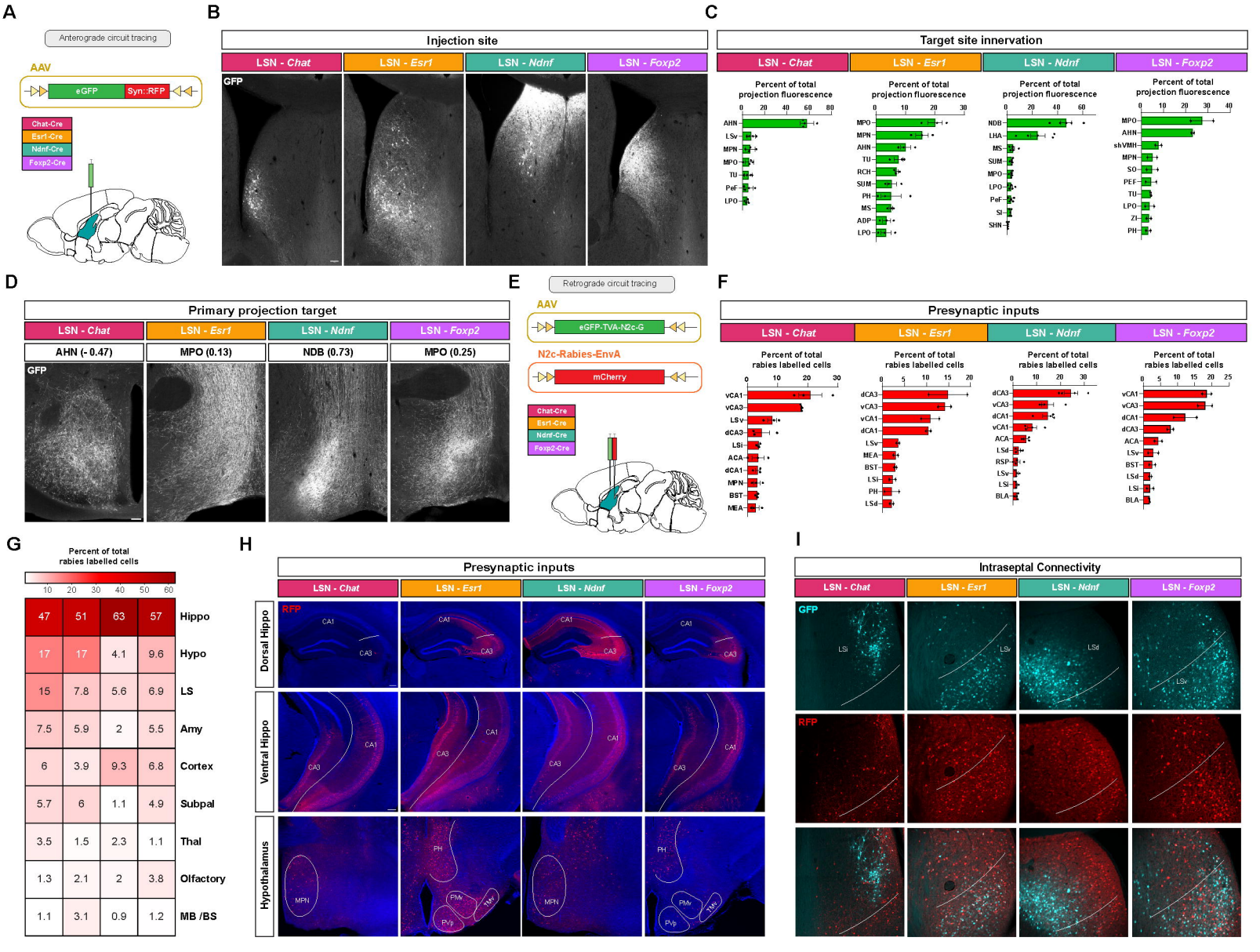
A
Anterograde circuit tracing
AAV
eGFP
Syn::RFP
Chat-Cre
Esr1-Cre
Ndnf-Cre
Foxp2-Cre
B
Injection site
LSN - Chat
LSN - Esr1
LSN - Ndnf
LSN - Foxp2
GFP
C
Target site innervation
LSN - Chat
LSN - Esr1
LSN - Ndnf
LSN - Foxp2
Percent of total projection fluorescence
AHN
LSv
MPN
MPO
TU
PeF
LPO
MPO
MPN
AHN
TU
RCH
SUM
PH
MS
ADP
LPO
NDB
LHA
MS
SUM
MPO
LPO
PeF
SI
SHN
MPO
AHN
shVMH
MPN
SO
PEF
TU
LPO
ZI
PH
D
Primary projection target
LSN - Chat
LSN - Esr1
LSN - Ndnf
LSN - Foxp2
AHN (- 0.47)
MPO (0.13)
NDB (0.73)
MPO (0.25)
GFP
E
Retrograde circuit tracing
AAV
eGFP-TVA-N2c-G
N2c-Rabies-EnvA
mCherry
Chat-Cre
Esr1-Cre
Ndnf-Cre
Foxp2-Cre
F
Presynaptic inputs
LSN - Chat
LSN - Esr1
LSN - Ndnf
LSN - Foxp2
Percent of total rabies labelled cells
vCA1
vCA3
LSv
dCA3
LSi
ACA
dCA1
MPN
BST
MEA
dCA3
vCA3
vCA1
dCA1
LSv
MEA
BST
LSi
PH
LSd
dCA3
vCA3
dCA1
vCA1
ACA
LSd
RSP
LSv
LSi
BLA
vCA1
vCA3
dCA1
dCA3
ACA
LSv
BST
LSd
LSi
BLA
G
Percent of total rabies labelled cells
10 20 30 40 50 60
47 51 63 57 Hippo
17 17 4.1 9.6 Hypo
15 7.8 5.6 6.9 LS
7.5 5.9 2 5.5 Amy
6 3.9 9.3 6.8 Cortex
5.7 6 1.1 4.9 Subpal
3.5 1.5 2.3 1.1 Thal
1.3 2.1 2 3.8 Olfactory
1.1 3.1 0.9 1.2 MB /BS
H
Presynaptic inputs
LSN - Chat
LSN - Esr1
LSN - Ndnf
LSN - Foxp2
Dorsal Hippo
Ventral Hippo
Hypothalamus
RFP
CA1
CA3
MPN
PH
PMv
PVp
TMv
I
Intraseptal Connectivity
LSN - Chat
LSN - Esr1
LSN - Ndnf
LSN - Foxp2
GFP
RFP
LSi
LSv
LSd
LSv

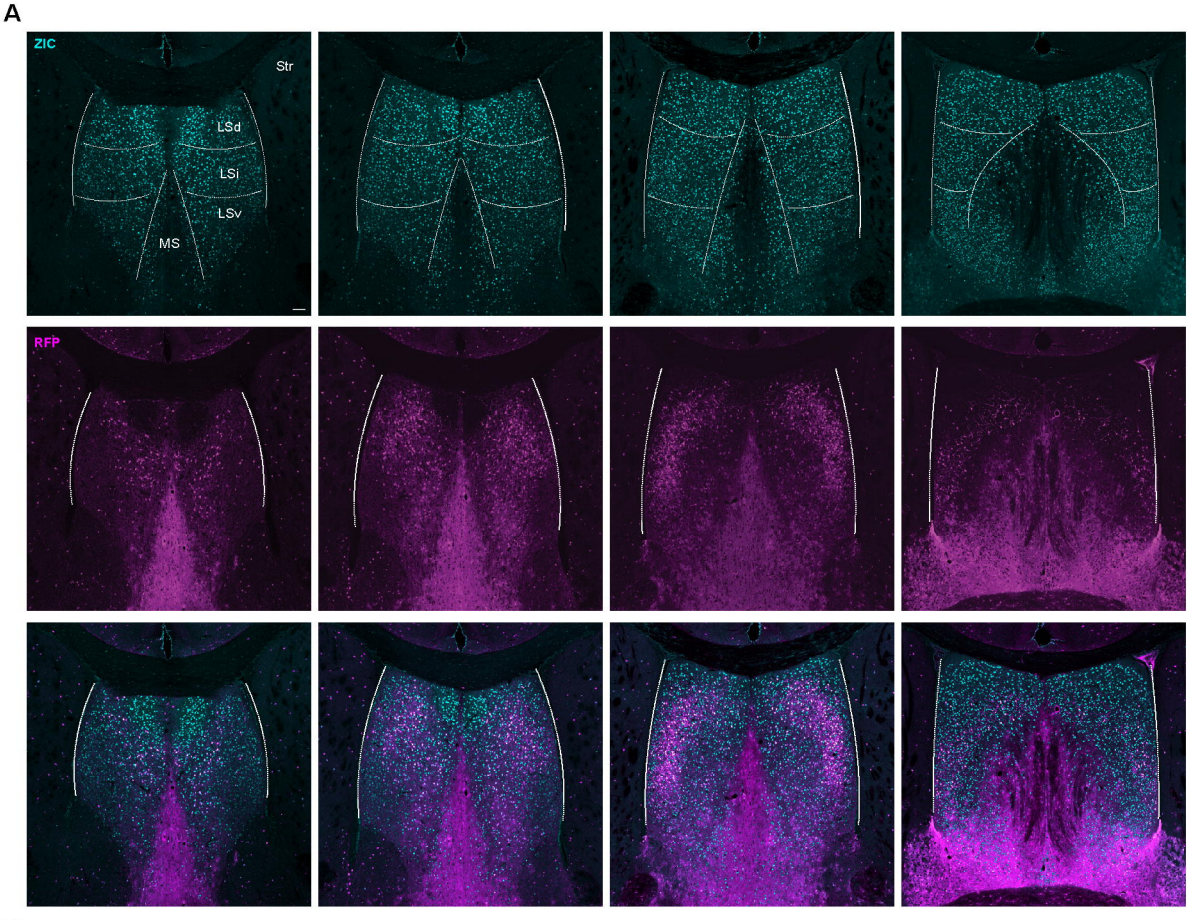
A
ZIC
Str
LSd
LSi
LSv
MS
RFP

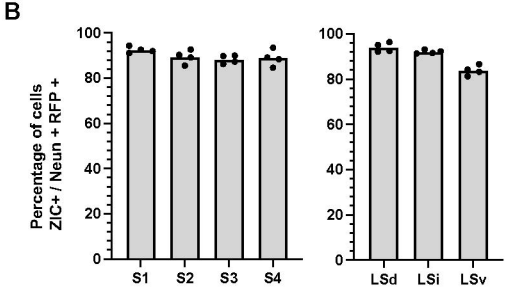
B
Percentage of cells
ZIC+ / Neun + RFP +
100
80
60
40
20
0
S1
S2
S3
S4
LSd
LSi
LSv

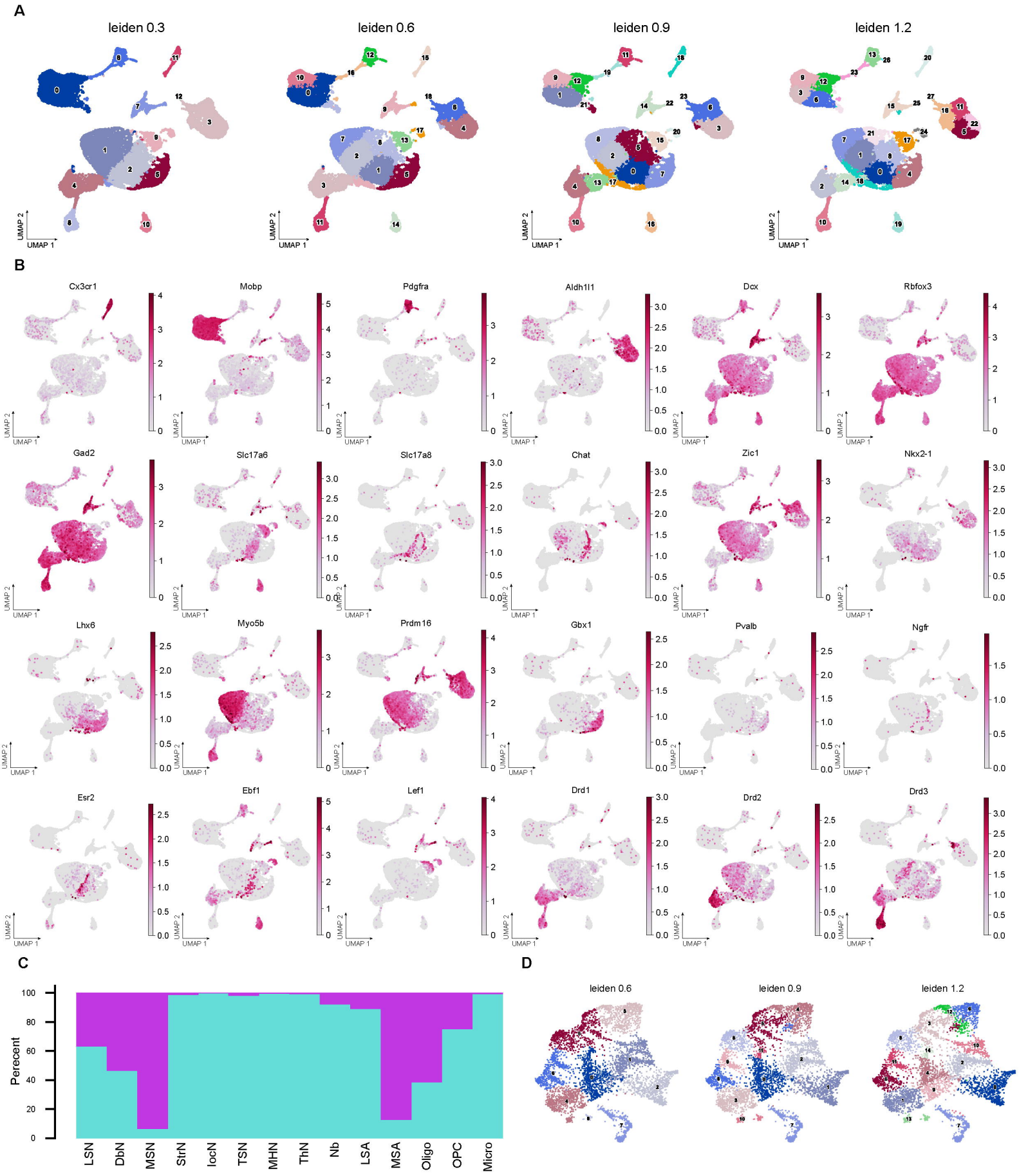
A
leiden 0.3
leiden 0.6
leiden 0.9
leiden 1.2
UMAP 1
UMAP 2
B
Cx3cr1
Mobp
Pdgfra
Aldh1l1
Dcx
Rbfox3
Gad2
Slc17a6
Slc17a8
Chat
Zic1
Nkx2-1
Lhx6
Myo5b
Prdm16
Gbx1
Pvalb
Ngfr
Esr2
Ebf1
Lef1
Drd1
Drd2
Drd3
C
Perecent
LSN
DbN
MSN
StrN
locN
TSN
MHN
ThN
Nb
LSA
MSA
Oligo
OPC
Micro
D
leiden 0.6
leiden 0.9
leiden 1.2

A

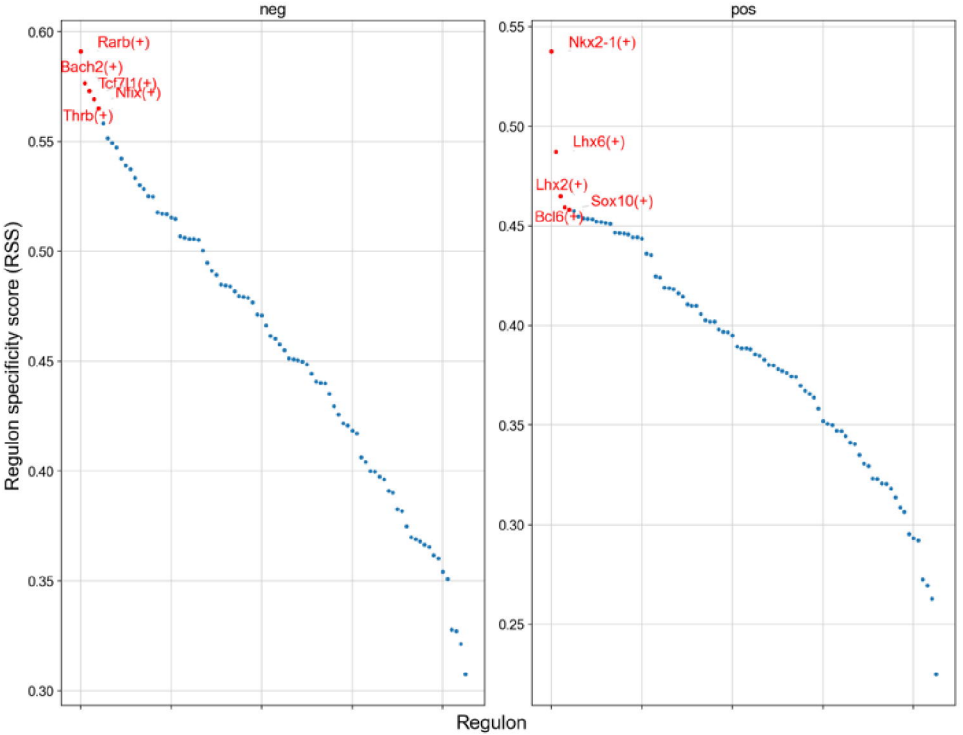
neg
pos
Rarb(+)
Bach2(+)
Tcf7l1(+)
Nfix(+)
Thrb(+)
Nkx2-1(+)
Lhx6(+)
Lhx2(+)
Sox10(+)
Bcl6(+)
Regulon specificity score (RSS)
Regulon
0.60
0.55
0.50
0.45
0.40
0.35
0.30
0.25

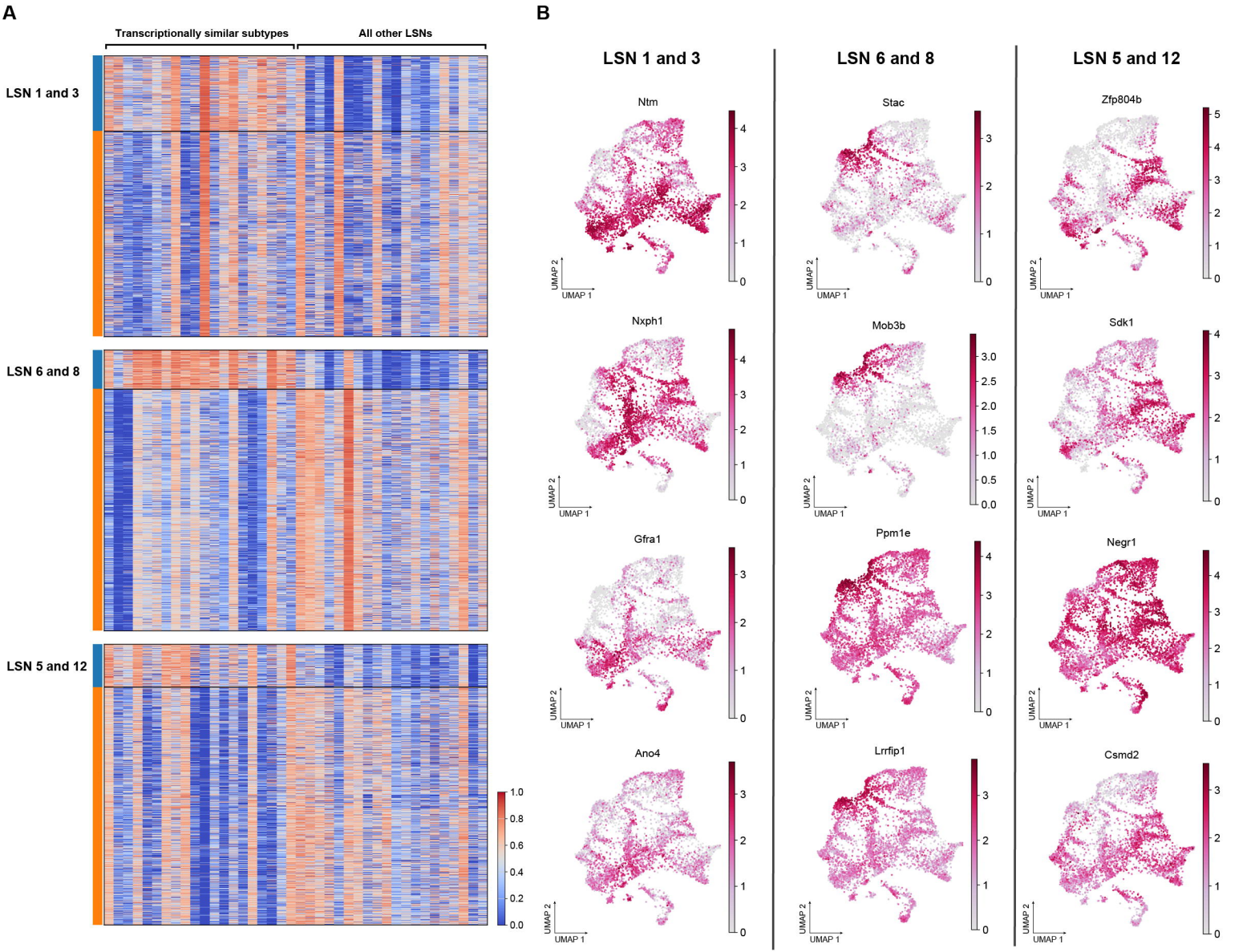
A
Transcriptionally similar subtypes
All other LSNs
LSN 1 and 3
LSN 6 and 8
LSN 5 and 12
1.0
0.8
0.6
0.4
0.2
0.0
B
LSN 1 and 3
LSN 6 and 8
LSN 5 and 12
Ntm
Stac
Zfp804b
Nxph1
Mob3b
Sdk1
Gfra1
Ppm1e
Negr1
Ano4
Lrrfip1
Csmd2
UMAP 1
UMAP 2

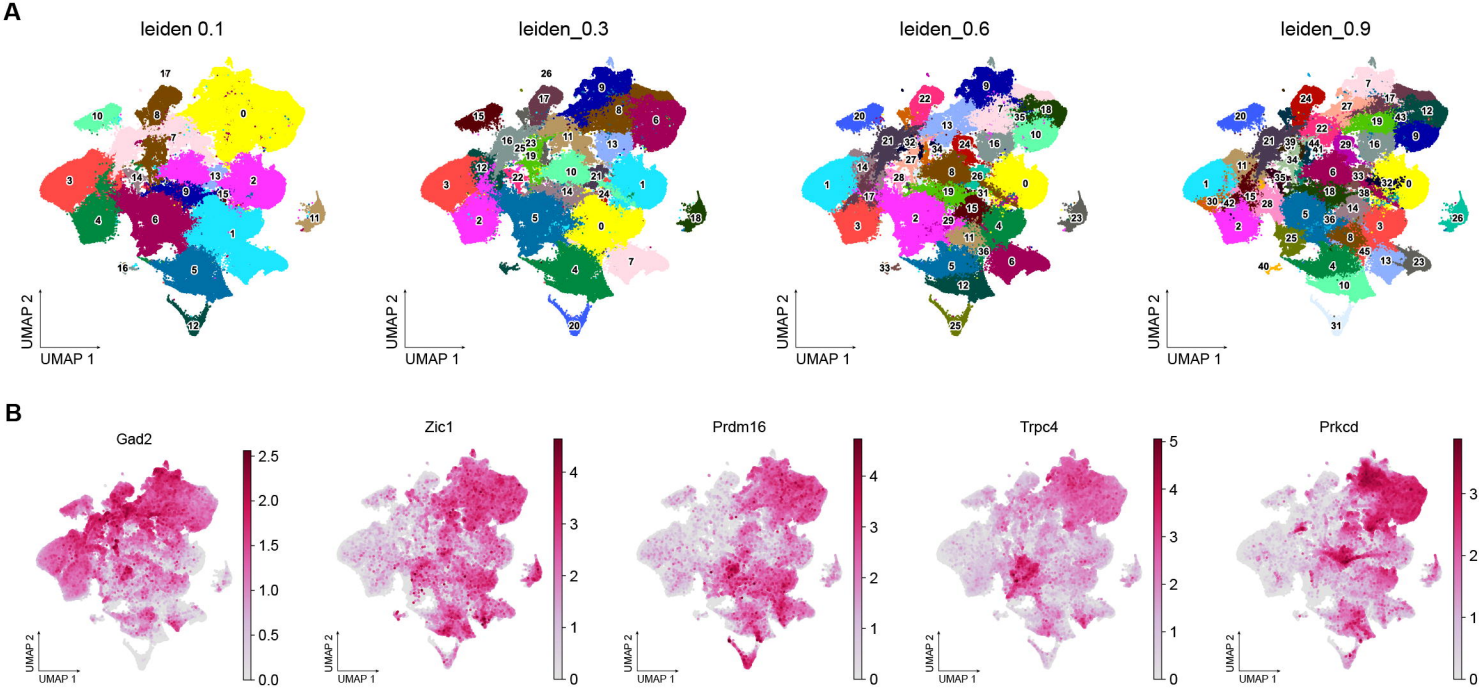
A
leiden 0.1
leiden_0.3
leiden_0.6
leiden_0.9
UMAP 2
UMAP 1
B
Gad2
Zic1
Prdm16
Trpc4
Prkcd

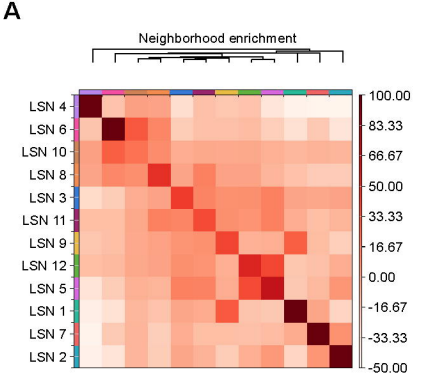
A
Neighborhood enrichment
LSN 4
LSN 6
LSN 10
LSN 8
LSN 3
LSN 11
LSN 9
LSN 12
LSN 5
LSN 1
LSN 7
LSN 2
100.00
83.33
66.67
50.00
33.33
16.67
0.00
-16.67
-33.33
-50.00

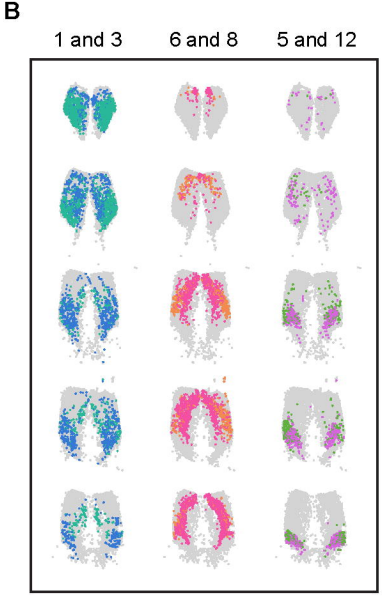
B
1 and 3
6 and 8
5 and 12

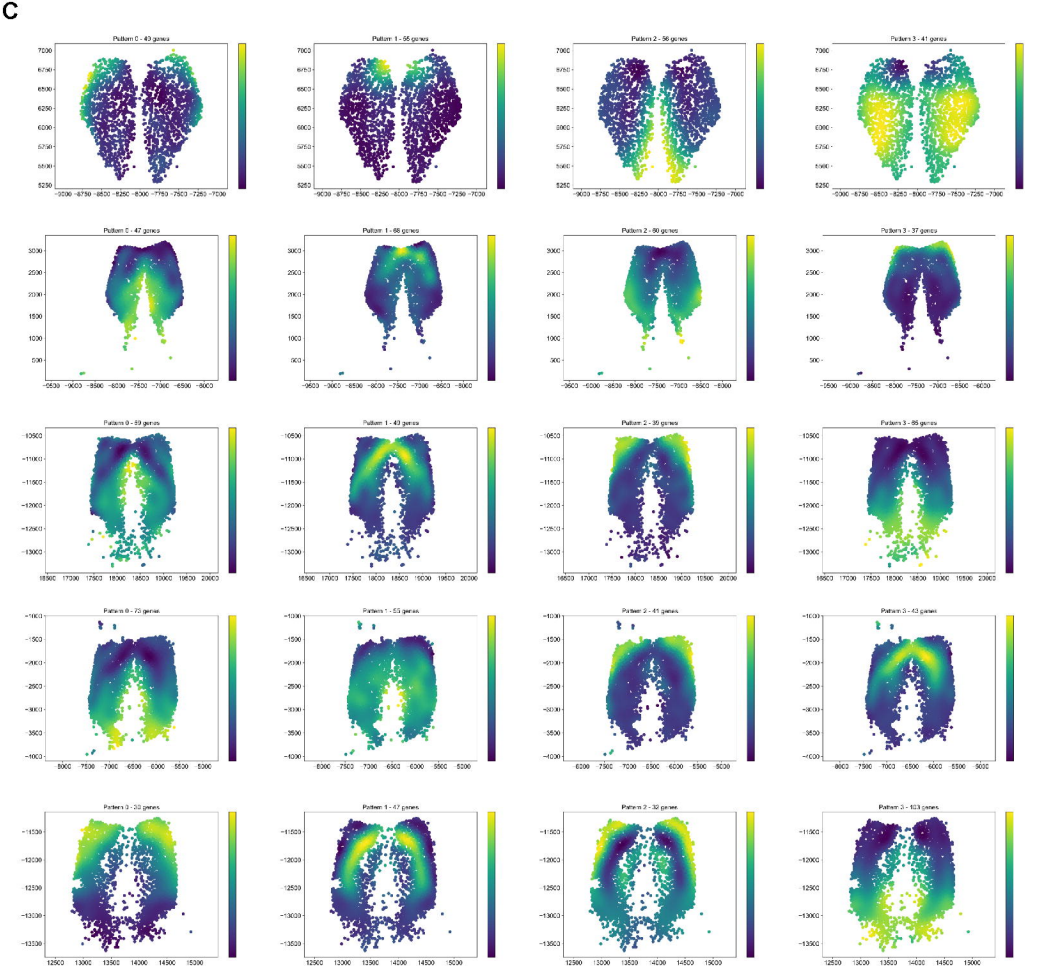
C